Remarkable Structural Diversity between Zr/Hf and Rare-Earth MOFs via Ligand Functionalization and the Discovery of Unique (4, 8)-c and (4, 12)-connected Frameworks

Giasemi K. Angeli[§], Danai Batzavali[§], Katerina Mavronasou[§], Constantinos Tsangarakis[§], Tobias Stuerzer[ǂ], Holger Ott[ǂ] and Pantelis N. Trikalitis[§,*]

[§]Department of Chemistry, University of Crete, Voutes 71003 Heraklion, Greece; [ǂ]Bruker AXS GmbH, Ostliche Rheinbruckenstr 49, D-76187 Karlsruhe, Germany

SUPPORTING INFORMATION

Table of Contents

Methods and Instrumentation

Starting Materials All chemicals were purchased commercially and were used without further purification. Hydrochloric acid 37%, $Pd(PPh_3)_4$, Acetone 99.5%, dichloromethane CH_2Cl_2, > 99.9%, c.H_2SO_4, chlorosulfonic acid 99%. Tetrahydrofuran (THF) >99.9%, methanol (MeOH) >99.8%, Ethanol absolute (EtOH) and H_3PO_2 50% in H_2O were purchased from Aldrich. N,N-Dimethylformamide 99.8%, $ZrCl_4$, $HfCl_4$, chlorotriphenyl methane 98%, isopentyl nitrite 97%, . $Y(NO_3)_3.6H_2O$ 99.9%, $Er(NO_3)_3.5H_2O$ 99.9% $Ho(NO_3)_3.5H_2O$ 99.9%, $Yb(NO_3)_3.5H_2O$ 99.9% and boronic acid were purchased from Alfa Aesar. Benzoic acid (reagent grade) was purchased from Riedel De Haeen.

Powder X-Ray Diffraction Patterns were collected using a Panalytical X'pert Pro MPD System Cu Kα (λ = 1.5418 A) radiation operated at 45 kV and 40 mA. A typical scan rate was 1.2 sec/step with a step size of 0.02 deg.

Single Crystal X-ray Diffraction

Single crystal X-ray diffraction data were collected on a Bruker D8 Venture diffractometer equipped with a Cu Incoatec microfocus IμS 3.0 source, a Photon II detector operating in shutterless mode and a cryostrem 800 system (Oxford Cryosystems) for temperature regulation.

Thermogravimetric analyses (TGA) were performed using a Shimadzu TA-50 instrument. An amount of 11.8 mg of sample was placed inside a quartz cap and heated up to 750^oC under N_2 flow with a heating rate of 5^oC/min.

^{1}H NMR spectra were recorded on a 500MHz Bruker spectrometer. MOF samples were prepared by digesting a small portion (~2mg) of the activated solids with a drop of concentrated HF or HCl acid (37%) in a DMSO-d_6 solution.

Gas Sorption Measurements. Low Pressure nitrogen, argon, carbon dioxide, methane and xenon gas sorption measurements were carried at different temperatures up to 1 bar using Autosorb-iQ2 instrument from Quantachrome equipped with a cryocooler system capable of temperature control from 20 to 320 K. In the case of M-**flu**-SO_2 (M: Zr, Hf), prior to analysis the as made sample was washed with N,N-dimethylformamide four times per day for 1 day and then soaked in acetone or dichloromethane 5 times per day for 6 days. Finally, the wet sample was transferred to a 6 mm sample cell and activated under dynamic vacuum at room temperature for 18 hours until the outgas rate was less than 2 mTorr/min. After evacuation the sample was weighted to obtain the precise mass of the evacuated sample and the cell was transferred to the analysis port of the gas sorption instrument. In the case of Y-**hpt**-MOF-1 and Y-**ken**-MOF-1 successful activation was achieved according to the following procedure: initially the solid was washed with fresh DMF (5 ml), three times per day for 2 days, to remove any unreacted starting materials from the pores. Then, DMF solvent was exchanged with ethanol (5 ml), four times per day for four days. After that the MOF was activated using a supercritical CO_2 under flow conditions, where ethanol was exchanged with liquid CO_2 for 24 hours using a flow of 0.5 ml per minute (20 ^oC and 1500 psi). Then, the sample was kept under supercritical CO_2 conditions (40 ^oC and 1500 psi) with a flow of 1 ml per minute, for 1 hour. Finally, CO_2 was slowly removed over a period of 5 hours using a needle valve. The activated sample was transferred in an Ar filled glove box, inserted in a 6 mm sample cell, transferred to the analysis station and evacuated under dynamic vacuum for 1 hour.

Organic Synthesis and ^{1}H NMR spectra

The tetrahedral carboxylate ligand H_4MTBC (4', 4'',4''',4''''-methanetetrayltetrabiphenyl-4-carboxylic acid) was synthesized according to previous literature reports with slight modifications.[1, 2] The precise synthetic procedure is described below (Scheme S1).

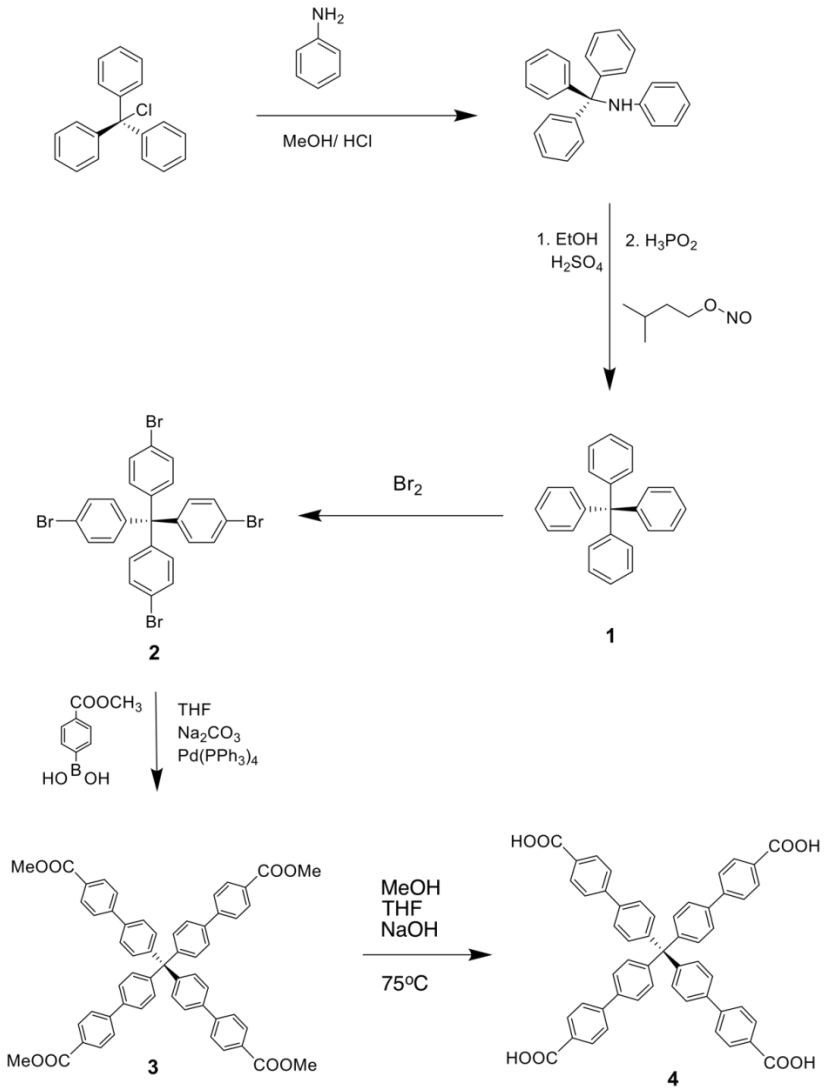

Scheme S1. Organic synthesis of H_4MTBC (**4**) ligand.

Compound 1. A 50 ml round bottom flask was loaded with 2 ml (22 mmol) aniline and 1 g (3.60 mmol) of chlorotriphenyl methane. This mixture was first heated at 200 ^{o}C for 5 min and then cooled to 90 ^{o}C where was held for 30 min. After that, 8 ml HCl 2N and 5 ml MeOH were added in the reaction mixture and stirred under reflux for 30 min. The resulting solid was filtrated, washed with a small amount of methanol (1-3 ml) and dissolved in 10 ml EtOH and 1 ml c.H_2SO_4. The system was cooled at -10 ^{o}C and 0.8 ml of isopentyl nitrite were added and stirred for 30 min. Then, 1.7 ml H_3PO_2 50% was added to the reaction mixture and left under reflux and stirring for 30 min. The resulting brown solid was filtrated and washed with EtOH. Yield: 1.1 g (95%), ^{1}H NMR (500 MHz, $CDCl_3$): 7.25 (m, 15H) (Figure S1).

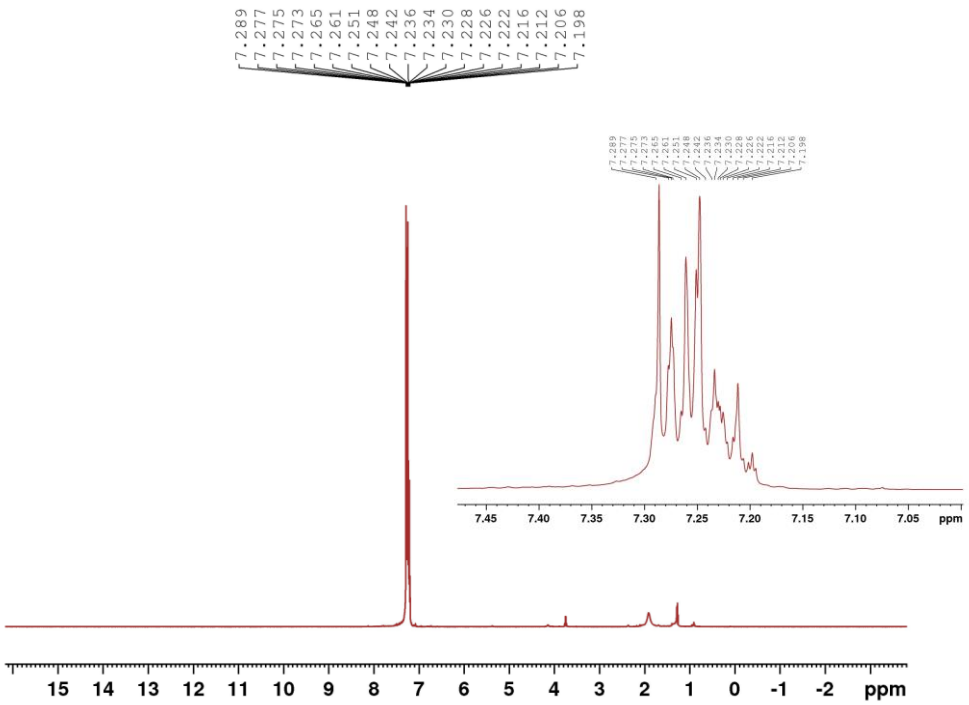

Figure S1. ^{1}HNMR spectrum of compound **1** in $CDCl_3$ (500MHz).

Compound 2. In a 25 ml round bottom flask compound **1** was added (1.1 g, 3.43 mmol) along with 5 ml of neat Br_2. The mixture was stirred for 60 min at room temperature. Then, chilled ethanol was added to the flask and a pale orange solid precipitates. This solid was filtrated and washed copiously with fresh ethanol. Yield: 1.58 g (72.4%) ^{1}H NMR (500 MHz, $CDCl_3$): 7.41 (d, J=8.5, 8H), 7.03 (d, J=8.5, 8H) (Figure S2).

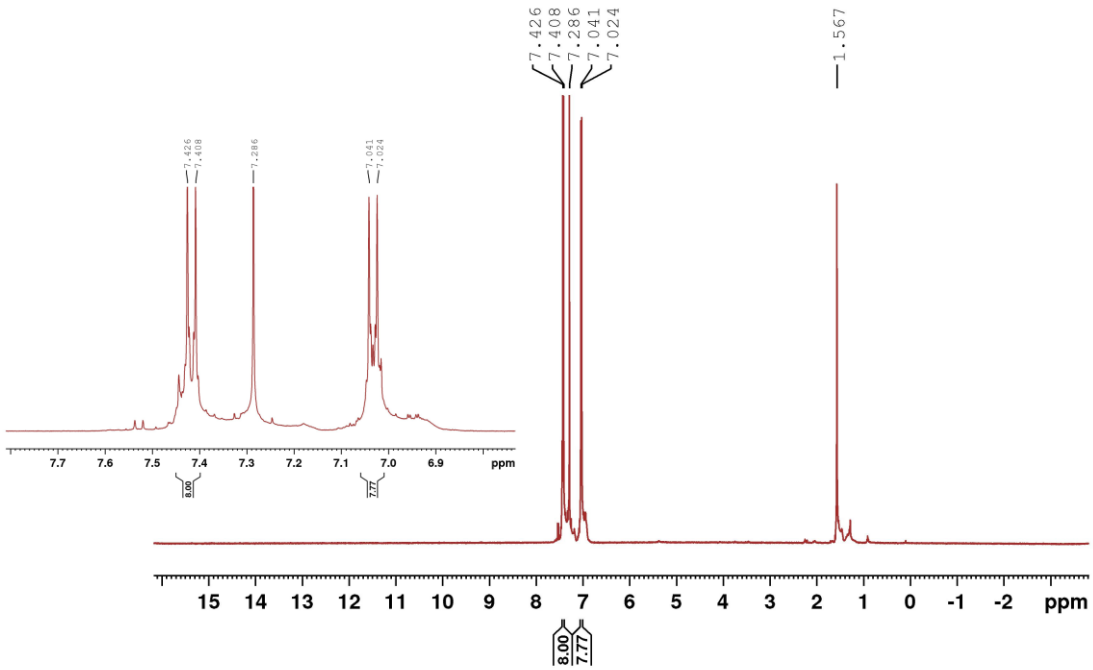

Figure S2. ^{1}HNMR spectrum of compound **2** in $CDCl_3$ (500 MHz).

Compound 3. In a dried under Ar double neck round bottom flask, 0.65 g of compound **2** (1 mmol) is added along with 40 ml of dry THF, 0.92 g (5.1 mmol) boronic ester, 20 ml Na_2CO_3 2M and 55 mg (0.047 mmol) $Pd(PPh_3)_4$. The system was sealed under Ar and refluxed for 5 days at 85 ^oC. After that period, the reaction mixture was extracted with THF which was then removed through rotary evaporation. The resulting solid was filtrated and washed copiously with water.

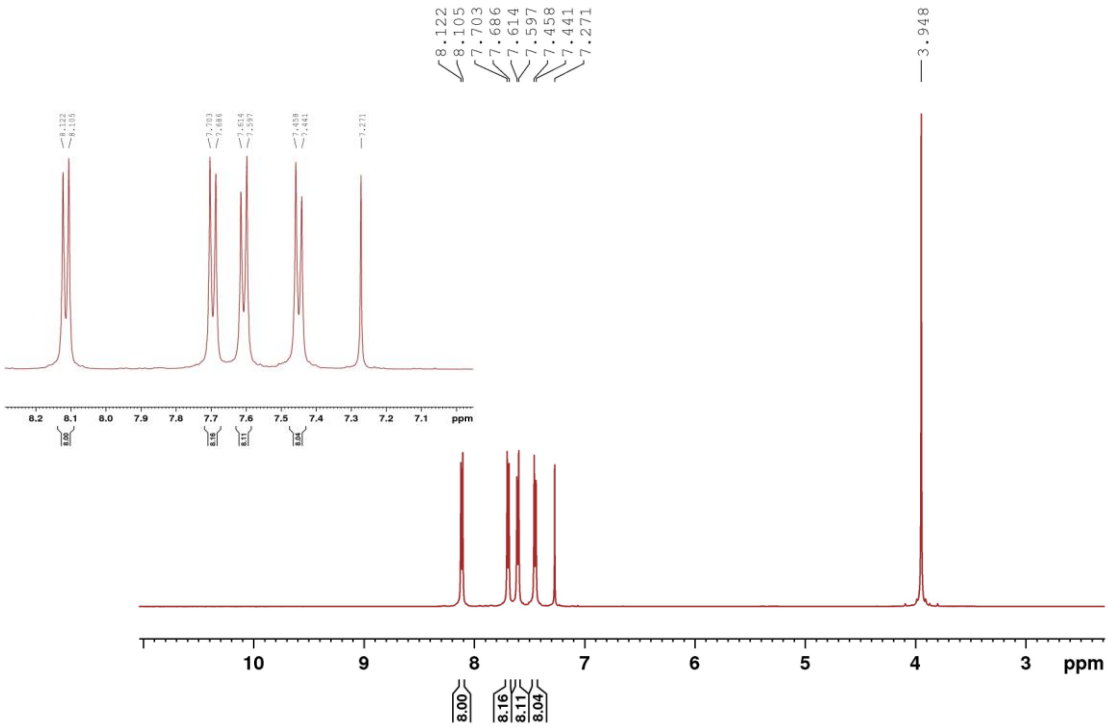

Figure S3. ^{1}HNMR spectrum of compound **3** in $CDCl_3$ (500MHz).

Compound 4. Compound **3** was added to a round bottom flask with 20 ml MeOH, 20 ml THF and 20 ml NaOH 5N. The mixture was refluxed at 85 ^oC overnight. After that period, 15 ml of HCl 3N were added to the reaction mixture and an off-white solid occurred. The solid was filtrated and then washed copiously with water and dried under vacuum. ^{1}H NMR (500 MHz, DMSO-d_6): 12.96 (br.s 2H), 8.00 (d, J=8Hz, 8H), 7.82 (d, J=8Hz, 8H), 7.76 (d. J=8Hz, 8H), 7.41(d, J=8Hz, 8H).

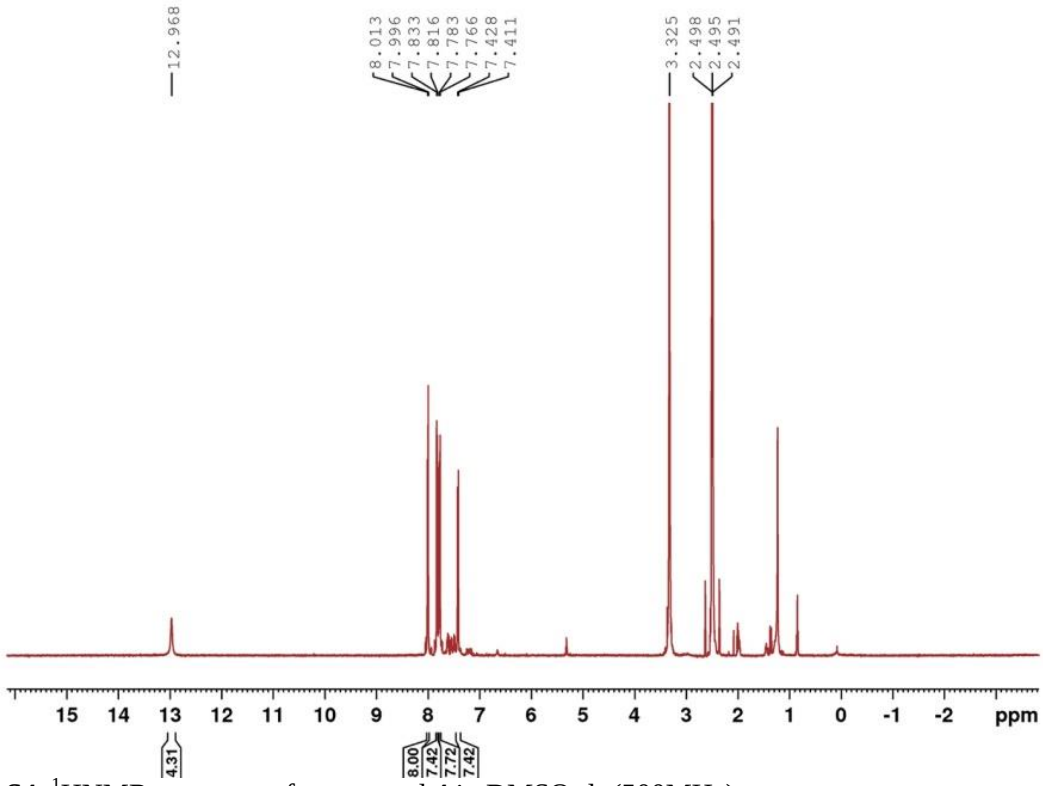

Figure S4. ^{1}HNMR spectrum of compound **4** in DMSO-d_6 (500MHz).

The sulfone functionalized H_4MTBC-SO_2 ligand (compound **5**) was synthesized according to the following procedure (Scheme S2).

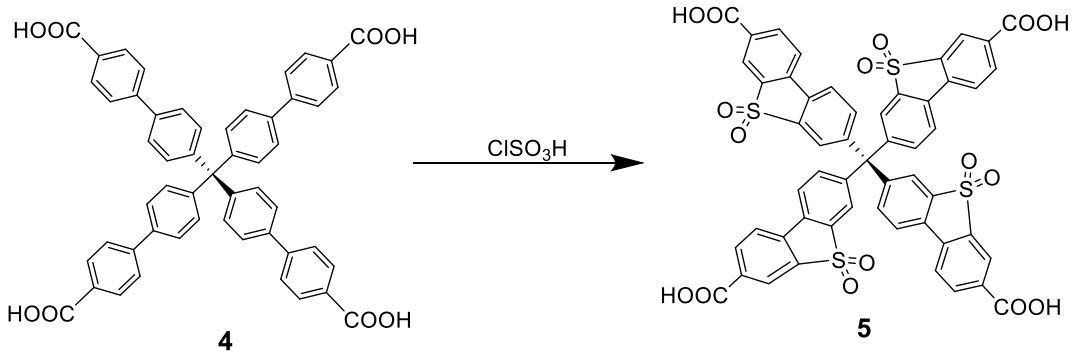

Scheme S2. Organic synthesis of the sulfone functionalized H_4MTBC-SO_2 (H_4**L2**) ligand.

Compound 5. A 25 ml round bottom flask was loaded with a 100 mg of compound **4**, then 5 ml $ClSO_3$ were added and the mixture was stirred at 145 ^{o}C for 60 min. After that the reaction mixture was neutralized by the addition of ice and the resulting dark red powder was washed copiously with water and dried at 90 ^{o}C. ^{1}H NMR (500 MHz, DMSO-d_6): 8.32 (m, 20H), 8 (d, J=8Hz, 4H).

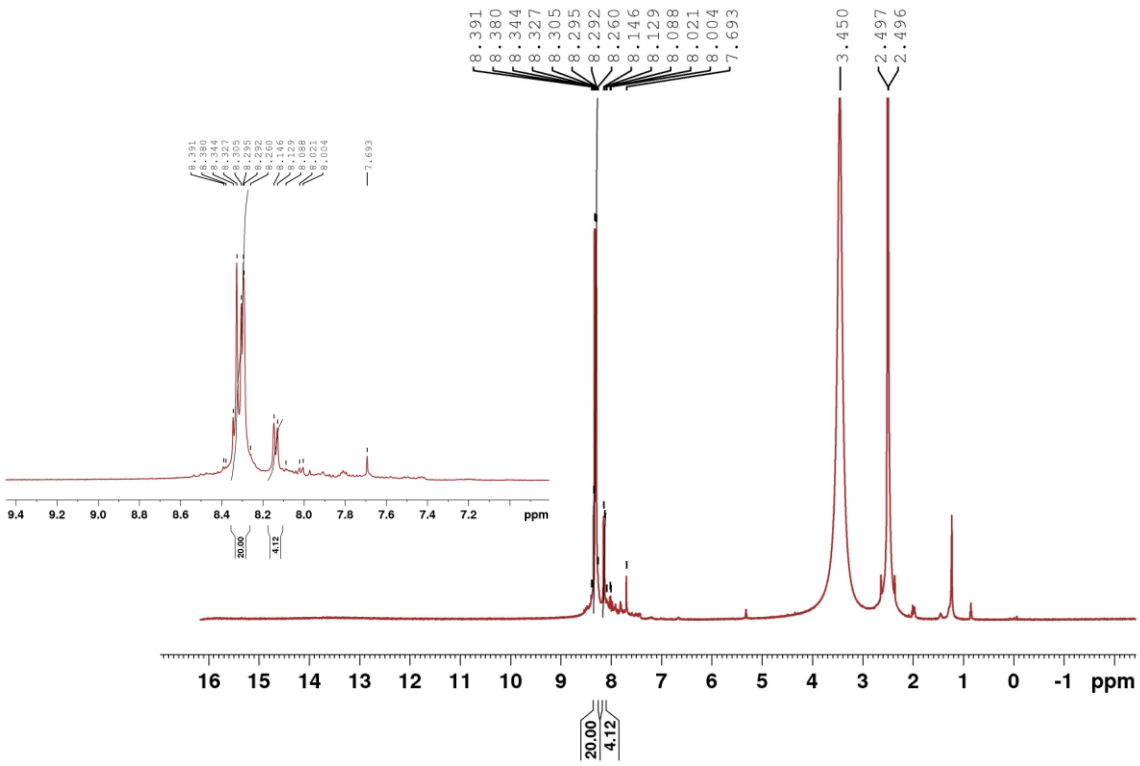

Figure S5. ^{1}HNMR spectrum of compound **5** in DMSO-d_6 (500MHz).

MOF Synthesis

Synthesis of Zr-**flu**-SO_2: A solution of 1.5 ml DMF, 450 mg benzoic acid, 0.0065 g (0.006 mmol) of H_4MTBC-SO_2 and 8.4 mg (0.036 mmol) of $ZrCl_4$ were placed in a 20 ml glass scintillation vial. The vial was sealed and placed in an isothermal oven at 120 ^oC for 12h. During this period, octahedral shaped light yellow crystals were formed. (50% yield based on H_4MBTC-SO_2).

Synthesis of Hf-**flu**-SO_2: A solution of 1.5 ml DMF, 450 mg benzoic acid, 0.0065 g (0.009 mmol) of H_4MTBC-SO_2 and 11.5 mg (0.036 mmol) of $HfCl_4$ were placed in a 20 ml glass scintillation vial. The vial was sealed and placed in an isothermal oven at 120 ^oC for 12h. During this period, octahedral shaped light yellow crystals were formed. (40% yield based on H_4MTBC-SO_2).

Synthesis of Y-**hpt**-MOF-1: A solution of 2.5 ml DMF, 250 mg 2-fluorobenzoic acid, 1ml acetic acid, 0.0082 g (0.0075 mmol) of H_4MTBC-SO_2 and 11.5 mg (0.03 mmol) of $Y(NO)_3.6H_2O$ were placed in a 20 ml glass scintillation vial. The vial was sealed and placed in an isothermal oven at 120 ^oC for 3 days. During this period, rhombohedral shaped yellow crystals were formed. (40% yield based on H_4MBTC-SO_2).

The above optimized conditions that afforded a high-quality product in a single crystal form, resulted after the exploration of a wide range of different synthetic parameters and summarized in the following table:

Table S1. Synthetic conditions explored for the identification of Y-**hpt**-MOF-1.

Metal-to-Ligand (M:L) molar ratio, range	DMF solvent	Modulators			
		2-FBA	CH_3COOH	2-FBA/CH_3COOH	HCOOH
3:1 to 8:1	1 to 3 ml	0.1 to 1 g	0.1 to 1 ml	(100 mg – 1 g)/(0.1 – 1 ml)	0.1 to 0.7 ml

The presence of acetic acid is crucial in obtaining a high-quality crystalline material because the use of only 2-FBA afforded the formation of Y-**hpt**-MOF-1 with low crystallinity as confirmed by PXRD and not in a single crystal form (see Figure S21). This solid was isolated using 600 mg of 2-FBA under otherwise similar reaction conditions.

Synthesis of Er-**hpt**-MOF-1**:** A solution of 2.5 ml DMF, 250 mg 2-flurobenzoic acid, 1ml acetic acid, 0.0082 g (0.0075 mmol) of H_4MTBC-SO_2 and 13.3 mg (0.03 mmol) of $Er(NO)_3.5H_2O$ were placed in a 20 ml glass scintillation vial. The vial was sealed and placed in an isothermal oven at 120 ^oC for 3 days. During this period, rhombohedral shaped light pink crystals were formed. (40% yield based on H_4MBTC-SO_2).

Synthesis of Ho-**hpt**-MOF-1**:** A solution of 2.5 ml DMF, 250 mg 2-fluorobenzoic acid, 1ml acetic acid, 0.0082 g (0.0075 mmol) of H_4MTBC-SO_2 and 13.2 mg (0.03 mmol) of $Ho(NO)_3.5H_2O$ were placed in a 20 ml glass scintillation vial. The vial was sealed and placed in an isothermal oven at 120 ^oC for 3 days. During this period, rhombohedral shaped pale orange crystals were formed. (40% yield based on H_4MBTC-SO_2).

Synthesis of Y-**ken**-MOF-1**:** A solution of 2.5 ml DMF, 250 mg 2-fluorobenzoic acid, 0.3 ml acetic acid, 0.006 g (0.0075 mmol) of H_4MTBC and 11 mg (0.03 mmol) of $Y(NO)_3.6H_2O$ were placed in a 20 ml glass scintillation vial. The vial was sealed and placed in an

isothermal oven at 120 ^{o}C for 3 days. During this period, hexagonal shaped pale yellow crystals were formed. (40% yield based on H_4MBTC).

Synthesis of Ho-**ken**-MOF-1**:** A solution of 2.5 ml DMF, 250 mg 2-fluorobenzoic acid, 0.3 ml acetic acid, 0.006 g (0.0075 mmol) of H_4MTBC and 11.5 mg (0.03 mmol) of $Ho(NO)_3.5H_2O$ were placed in a 20 ml glass scintillation vial. The vial was sealed and placed in an isothermal oven at 120 ^{o}C for 3 days. During this period, hexagonal shaped pale pink crystals were formed. (40% yield based on H_4MBTC).

Synthesis of Er-**ken**-MOF-1**:** A solution of 2.5 ml DMF, 250 mg 2-fluorobenzoic acid, 0.3 ml acetic acid, 0.006 g (0.0075 mmol) of H_4MTBC and 11.5 mg (0.03 mmol) of $Er(NO)_3.5H_2O$ were placed in a 20 ml glass scintillation vial. The vial was sealed and placed in an isothermal oven at 120 ^{o}C for 3 days. During this period, hexagonal shaped pink crystals were formed. (40% yield based on H_4MBTC).

Synthesis of Yb-**ken**-MOF-1**:** A solution of 2.5 ml DMF, 250 mg 2-fluorobenzoic acid, 0.3 ml acetic acid, 0.006 g (0.0075 mmol) of H_4MTBC and 11.5 mg (0.03 mmol) of $Yb(NO)_3.6H_2O$ were placed in a 20 ml glass scintillation vial. The vial was sealed and placed in an isothermal oven at 120 ^{o}C for 3 days. During this period, small hexagonal shaped colorless crystals were formed. (40% yield based on H_4MBTC).

Scanning Electron Microscopy (SEM) Images

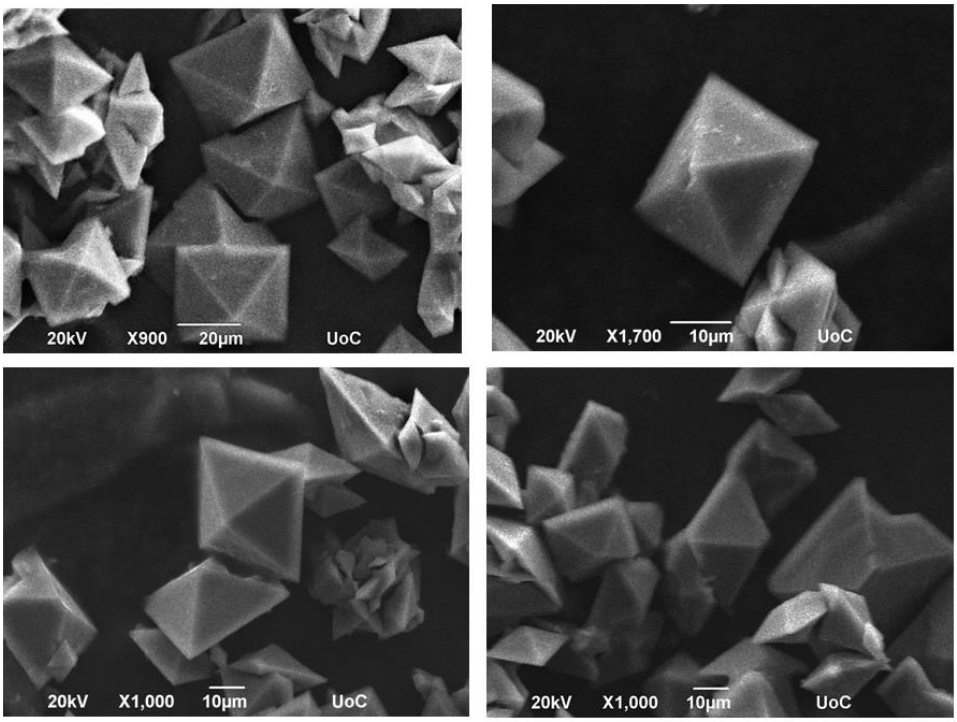

Figure S6. Scanning Electron Microscopy (SEM) images of the as made Zr-**flu**-SO_2 (top) and Hf-**flu**-SO_2 (bottom).

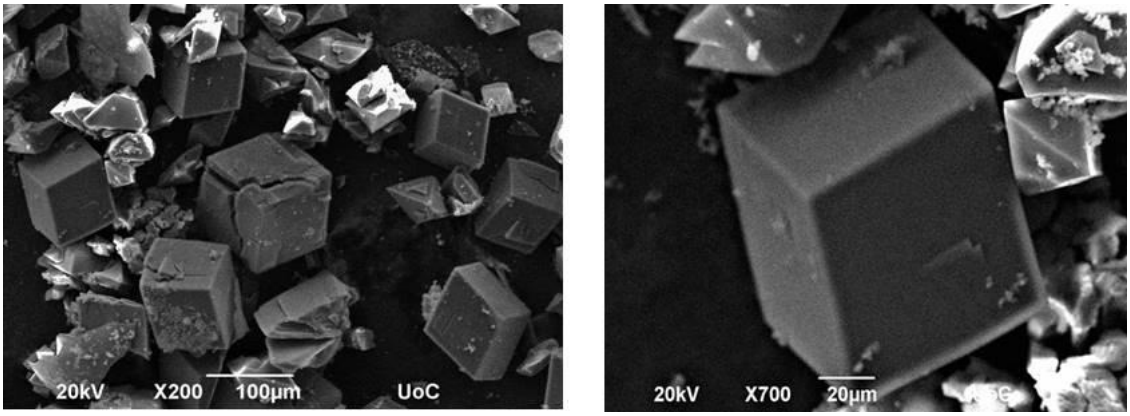

Figure S7. SEM images of the as-made Y-**hpt**-MOF-1 single crystals.

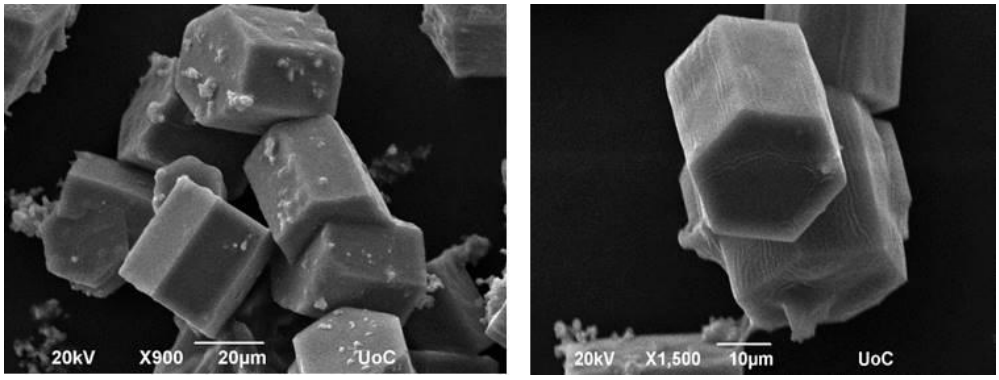

Figure S8. SEM images of as-made Y-**ken**-MOF-1 single crystals.

Single crystal X-ray crystallography and structural figures

Data for Zr-**flu**-SO_2

A total of 781 frames were collected. The total exposure time was 7.81 hours. The frames were integrated with the Bruker SAINT software package using a narrow-frame algorithm. The integration of the data using a tetragonal unit cell yielded a total of 88583 reflections to a maximum θ angle of 54.38° (0.95 Å resolution), of which 5902 were independent (average redundancy 15.009, completeness = 99.6%, R_{int} = 9.51%, R_{sig} = 4.55%) and 4581 (77.62%) were greater than $2\sigma(F^2)$. The final cell constants of a = 24.6334(16) Å, b = 24.6334(16) Å, c = 29.830(2) Å, volume = 18101.(3) $Å^3$, are based upon the refinement of the XYZ-centroids of 9873 reflections above 20 σ(I) with 8.024° < 2θ < 108.7°. Data were corrected for absorption effects using the Multi-Scan method (SADABS). The ratio of minimum to maximum apparent transmission was 0.563. The calculated minimum and maximum transmission coefficients (based on crystal size) are 0.0090 and 0.0110.

The structure was solved and refined using the Bruker SHELXTL Software Package, using the space group P 42/m n m, with Z = 2 for the formula unit, $C_{106}H_{48}O_{48}S_8Zr_6$. The final anisotropic full-matrix least-squares refinement on $F^2$with 199 variables converged at R1 = 12.98%, for the observed data and wR2 = 40.21% for all data. The goodness-of-fit was 1.729. The largest peak in the final difference electron density synthesis was 1.439 $e^-/Å^3$ and the largest hole was -0.850 $e^-/Å^3$ with an RMS deviation of 0.191 $e^-/Å^3$. On the basis of the final model, the calculated density was 0.531 g/cm^3 and F(000), 2872 e^-. CCDC No.: 2012455.

Table S2. Sample and crystal data for Zr-**flu**-SO_2.

Identification code	Zr-**flu**-SO_2	
Chemical formula	$C_{106}H_{48}O_{48}S_8Zr_6$	
Formula weight	2893.24 g/mol	
Temperature	200(2) K	
Wavelength	1.54184 Å	
Crystal size	0.025 x 0.025 x 0.040 mm	
Crystal system	Tetragonal	
Space group	P 4_2/m n m	
Unit cell dimensions	a = 24.6334(16) Å	α = 90°
	b = 24.6334(16) Å	β = 90°
	c = 29.830(2) Å	γ = 90°
Volume	18101.(3) $Å^3$	
Z	2	
Density (calculated)	0.531 g/cm^3	
Absorption coefficient	2.052 mm^{-1}	
F(000)	2872	
Theta range for data collection	2.94 to 54.38°	
Index ranges	-24<=h<=25, -25<=k<=21, -31<=l<=30	
Reflections collected	88583	
Independent reflections	5902 [R(int) = 0.0951]	
Coverage of independent reflections	99.6%	
Absorption correction	Multi-Scan	
Max. and min. transmission	0.0110 and 0.0090	
Structure solution technique	direct methods	
Structure solution program	SHELXT 2014/5 (Sheldrick, 2014)	
Refinement method	Full-matrix least-squares on F^2	
Refinement program	SHELXL-2018/3 (Sheldrick, 2018)	
Function minimized	$\Sigma\, w(F_o^2 - F_c^2)^2$	
Data / restraints / parameters	5902 / 0 / 199	
Goodness-of-fit on F^2	1.729	
Δ/σ_{max}	0.004	
Final R indices	4581 data; I>2σ(I)	R1 = 0.1298, wR2 = 0.3792
	all data	R1 = 0.1483, wR2 = 0.4021
Weighting scheme	$w=1/[\sigma^2(F_o^2)+(0.2000P)^2]$ where $P=(F_o^2+2F_c^2)/3$	
Largest diff. peak and hole	1.439 and -0.850 $eÅ^{-3}$	
R.M.S. deviation from mean	0.191 $eÅ^{-3}$	

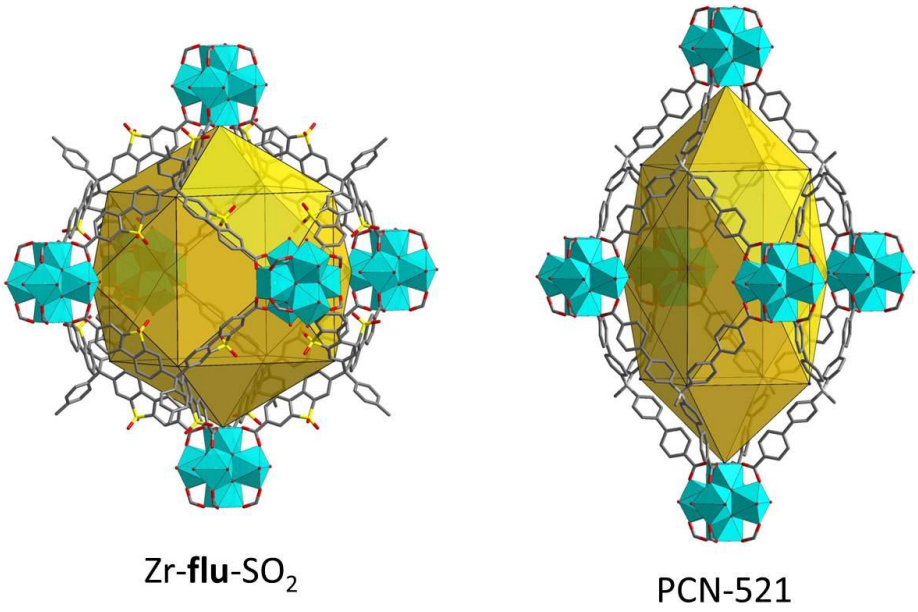

Figure S9. The polyhedral cavity in Zr-**flu**-SO_2 (left) and PCN-521 (right).

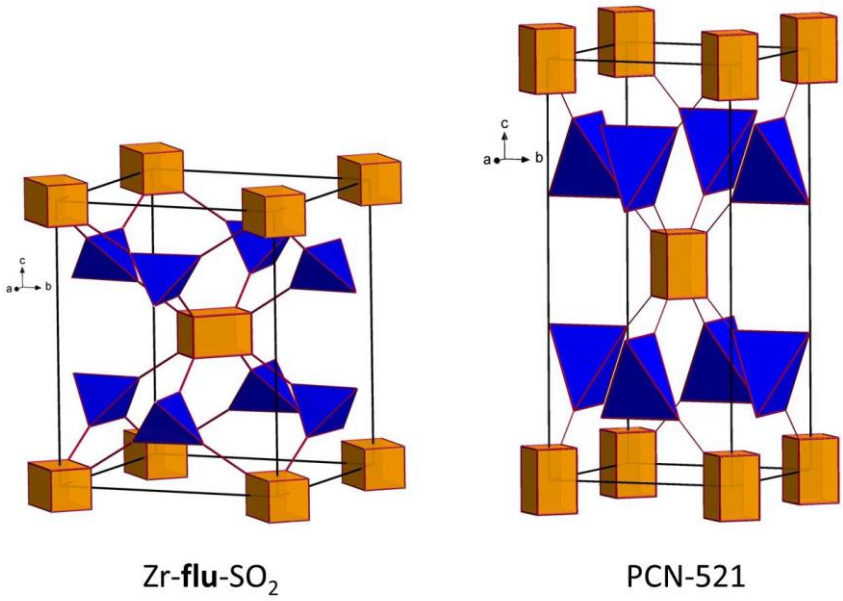

Figure S10. The **flu**-a net in Zr-**flu**-SO_2 (left) and PCN-521 (right). Note that in Zr-**flu**-SO_2 the central Zr_6-cluster is rotated by 90° around the c-axis relative to those at the corners, where in PCN-521 all clusters have the same relative positioning.

Data for Hf-**flu**-SO_2

A total of 1564 frames were collected. The total exposure time was 25.28 hours. The frames were integrated with the Bruker SAINT software package using a narrow-frame algorithm. The integration of the data using a tetragonal unit cell yielded a total of 89136 reflections to a maximum θ angle of 55.37° (0.94 Å resolution), of which 5936 were independent (average redundancy 15.016, completeness = 97.1%, R_{int} = 10.20%, R_{sig} = 4.44%) and 4569 (76.97%) were greater than $2\sigma(F^2)$. The final cell constants of a = 23.955(2) Å, b = 23.955(2) Å, c = 31.402(4) Å, volume = 18020.(4) $Å^3$, are based upon the refinement of the XYZ-centroids of 9469 reflections above 20 σ(I) with 4.639° < 2θ < 108.2°. Data were corrected for absorption effects using the Multi-Scan method (SADABS). The ratio of minimum to maximum apparent transmission was 0.733. The

calculated minimum and maximum transmission coefficients (based on crystal size) are 0.8790 and 0.9120.

The structure was solved and refined using the Bruker SHELXTL Software Package, using the space group P 42/m n m, with Z = 2 for the formula unit, $C_{106}H_{48}Hf_6O_{48}S_8$. The final anisotropic full-matrix least-squares refinement on F^2 with 199 variables converged at R1 = 9.95%, for the observed data and wR2 = 33.13% for all data. The goodness-of-fit was 1.347. The largest peak in the final difference electron density synthesis was 1.571 $e^-/Å^3$ and the largest hole was -1.434 $e^-/Å^3$ with an RMS deviation of 0.208 $e^-/Å^3$. On the basis of the final model, the calculated density was 0.630 g/cm^3 and F(000), 3256 e^-. CCDC No.: 2012452.

Table S3. Sample and crystal data for Hf-**flu**-SO_2.

Chemical formula	$C_{106}H_{48}Hf_6O_{48}S_8$	
Formula weight	3416.86 g/mol	
Temperature	200(2) K	
Wavelength	1.54178 Å	
Crystal size	0.025 x 0.025 x 0.035 mm	
Crystal system	tetragonal	
Space group	P 4_2/m n m	
Unit cell dimensions	a = 23.955(2) Å	α = 90°
	b = 23.955(2) Å	β = 90°
	c = 31.402(4) Å	γ = 90°
Volume	18020.(4) $Å^3$	
Z	2	
Density (calculated)	0.630 g/cm^3	
Absorption coefficient	3.773 mm^{-1}	
F(000)	3256	
Theta range for data collection	2.32 to 55.37°	
Index ranges	-25<=h<=21, -23<=k<=25, -33<=l<=33	
Reflections collected	89136	
Independent reflections	5936 [R(int) = 0.1020]	
Coverage of independent reflections	97.1%	
Absorption correction	Multi-Scan	
Max. and min. transmission	0.9120 and 0.8790	
Structure solution technique	direct methods	
Structure solution program	SHELXT 2014/5 (Sheldrick, 2014)	
Refinement method	Full-matrix least-squares on F^2	
Refinement program	SHELXL-2018/3 (Sheldrick, 2018)	
Function minimized	$\Sigma\, w(F_o^2 - F_c^2)^2$	
Data / restraints / parameters	5936 / 0 / 199	
Goodness-of-fit on F^2	1.347	
Δ/σ_{max}	0.004	
Final R indices	4569 data; I>2σ(I)	R1 = 0.0995, wR2 = 0.3146
	all data	R1 = 0.1133, wR2 = 0.3313
Weighting scheme	$w=1/[\sigma^2(F_o^2)+(0.2000P)^2]$ where $P=(F_o^2+2F_c^2)/3$	
Largest diff. peak and hole	1.571 and -1.434 $eÅ^{-3}$	

R.M.S. deviation from mean	0.208 eÅ^{-3}

Data for Y-**hpt**-MOF-1

A total of 1023 frames were collected. The total exposure time was 5.68 hours. The frames were integrated with the Bruker SAINT software package using a narrow-frame algorithm. The integration of the data using a trigonal unit cell yielded a total of 60018 reflections to a maximum θ angle of 45.19° (1.09 Å resolution), of which 6367 were independent (average redundancy 9.426, completeness = 99.7%, R_{int} = 3.87%, R_{sig} = 2.05%) and 5615 (88.19%) were greater than 2σ(F^2). The final cell constants of a = 39.5393(14) Å, b = 39.5393(14) Å, c = 48.8586(19) Å, volume = 66150.(5) Å^3, are based upon the refinement of the XYZ-centroids of 9927 reflections above 20 σ(I) with 5.427° < 2θ < 94.91°. Data were corrected for absorption effects using the Multi-Scan method (SADABS). The ratio of minimum to maximum apparent transmission was 0.764. The structure was solved and refined using the Bruker SHELXTL Software Package, using the space group R -3 m, with Z = 6 for the formula unit, $C_{161}H_{75}O_{71}S_{12}Y_9$. The final anisotropic full-matrix least-squares refinement on F^2 with399 variables converged at R1 = 14.53%, for the observed data and wR2 = 44.81% for all data. The goodness-of-fit was 2.223. The largest peak in the final difference electron density synthesis was 2.416 e$^-$/Å^3 and the largest hole was -0.805 e$^-$/Å^3 with an RMS deviation of 0.228 e$^-$/Å^3. On the basis of the final model, the calculated density was 0.652 g/cm^3 and F(000), 12912 e$^-$. CCDC No.: 2012453.

Table S4. Sample and crystal data for Y-**hpt**-MOF-1.

Identification code	Y-**hpt**-MOF-1	
Chemical formula	$C_{161}H_{75}O_{71}S_{12}Y_9$	
Formula weight	4330.12 g/mol	
Temperature	200(2) K	
Wavelength	1.54178 Å	
Crystal system	trigonal	
Space group	R -3 m	
Unit cell dimensions	a = 39.5393(14) Å	α = 90°
	b = 39.5393(14) Å	β = 90°
	c = 48.8586(19) Å	γ = 120°
Volume	66150.(5) Å^3	
Z	6	
Density (calculated)	0.652 g/cm^3	
Absorption coefficient	2.362 mm^{-1}	
F(000)	12912	
Theta range for data collection	2.71 to 45.19°	
Index ranges	-36<=h<=31, -26<=k<=36, -44<=l<=44	
Reflections collected	60018	
Independent reflections	6367 [R(int) = 0.0387]	
Coverage of independent reflections	99.7%	
Absorption correction	Multi-Scan	
Structure solution technique	direct methods	
Structure solution program	SHELXT 2014/5 (Sheldrick, 2014)	
Refinement method	Full-matrix least-squares on F^2	
Refinement program	SHELXL-2018/3 (Sheldrick, 2018)	

Function minimized	$\Sigma w(F_o^2 - F_c^2)^2$	
Data / restraints / parameters	6367 / 21 / 399	
Goodness-of-fit on F^2	2.223	
Δ/σ_{max}	0.002	
Final R indices	5615 data; $I>2\sigma(I)$	R1 = 0.1453, wR2 = 0.4360
	all data	R1 = 0.1525, wR2 = 0.4481
Weighting scheme	$w=1/[\sigma^2(F_o^2)+(0.2000P)^2]$ where $P=(F_o^2+2F_c^2)/3$	
Largest diff. peak and hole	2.416 and -0.805 eÅ^{-3}	
R.M.S. deviation from mean	0.228 eÅ^{-3}	

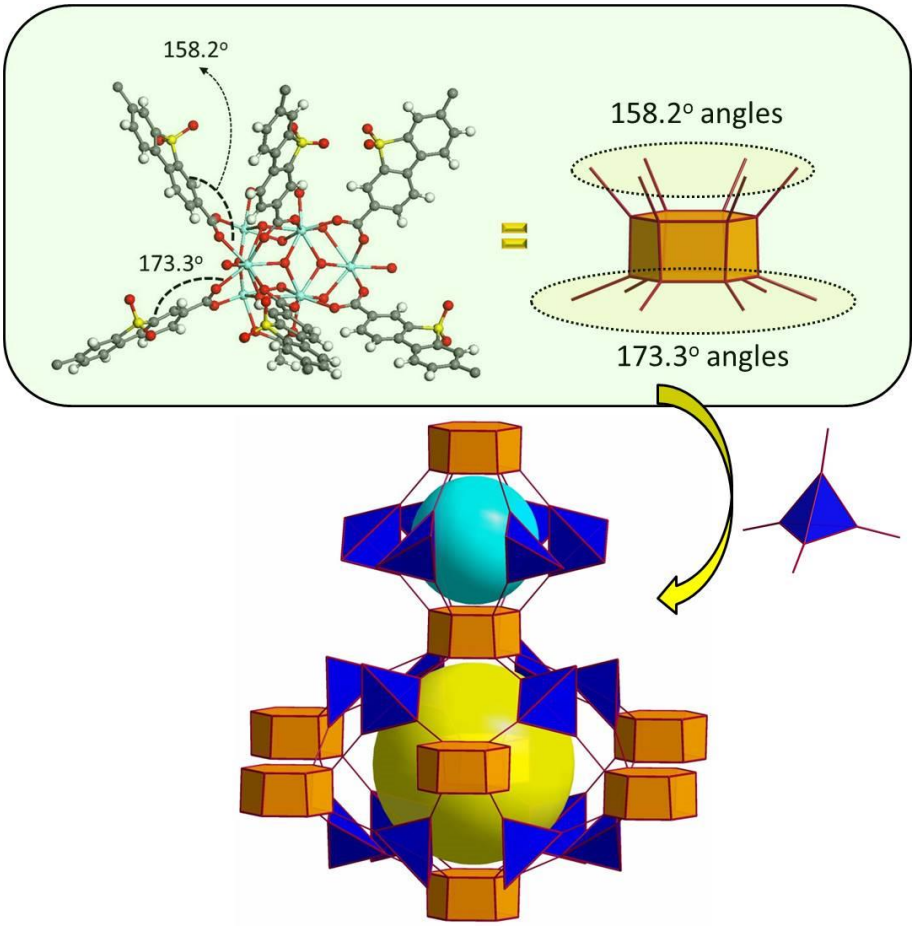

Figure S11. The different coordination angles of the linkers above and below the nonanuclear hexagonal prismatic Y-cluster, results in the formation of two different cavities shown with a light blue and a yellow sphere.

Data for Er-**hpt**-MOF-1.

A specimen of $C_{163}H_{75}Er_9O_{71}S_{12}$, approximate dimensions 0.025 mm x 0.050 mm x 0.050 mm, was used for the X-ray crystallographic analysis. The X-ray intensity data were measured (λ = 1.54178 Å). The integration of the data using a trigonal unit cell yielded a total of 76146 reflections to a maximum θ angle of 44.53° (1.10 Å resolution), of which 6153 were independent (average redundancy 12.375, completeness = 99.8%, R_{int} =3.81%, R_{sig} = 1.76%)

and 5467 (88.85%) were greater than $2\sigma(F^2)$. The final cell constants of a = 39.524(2) Å, b = 39.524(2) Å, c = 48.846(3) Å, volume = 66082.(8) $Å^3$, are based upon the refinement of the XYZ-centroids of reflections above 20 σ(I). The calculated minimum and maximum transmission coefficients (based on crystal size) are 0.8300 and 0.9090. The final anisotropic full-matrix least-squares refinement on F^2 with 405 variables converged at R1 = 10.16%, for the observed data and wR2 = 36.35% for all data. The goodness-of-fit was 1.781. The largest peak in the final difference electron density synthesis was 4.106 $e^-/Å^3$ and the largest hole was -0.956 $e^-/Å^3$ with an RMS deviation of 0.211 $e^-/Å^3$. On the basis of the final model, the calculated density was 0.763 g/cm^3 and F(000), 14550 e^-. CCDC No.: 2012451.

Table S5. Sample and crystal data for Er-**hpt**-MOF-1.

Identification code	Er-**hpt**-MOF-1	
Chemical formula	$C_{163}H_{75}Er_9O_{71}S_{12}$	
Formula weight	5059.29 g/mol	
Temperature	200(2) K	
Wavelength	1.54178 Å	
Crystal size	0.025 x 0.050 x 0.050 mm	
Crystal system	trigonal	
Space group	R -3 m	
Unit cell dimensions	a = 39.524(2) Å	α = 90°
	b = 39.524(2) Å	β = 90°
	c = 48.846(3) Å	γ = 120°
Volume	66082.(8) $Å^3$	
Z	6	
Density (calculated)	0.763 g/cm^3	
Absorption coefficient	3.870 mm^{-1}	
F(000)	14550	
Theta range for data collection	2.71 to 44.53°	
Index ranges	-35<=h<=35, -35<=k<=35, -44<=l<=44	
Reflections collected	76146	
Independent reflections	6153 [R(int) = 0.0381]	
Max. and min. transmission	0.9090 and 0.8300	
Refinement method	Full-matrix least-squares on F^2	
Refinement program	SHELXL-2018/3 (Sheldrick, 2018)	
Function minimized	$\Sigma w(F_o^2 - F_c^2)^2$	
Data / restraints / parameters	6153 / 43 / 405	
Goodness-of-fit on F^2	1.781	
Δ/σ_{max}	0.002	
Final R indices	5467 data; I>2σ(I)	R1 = 0.1016, wR2 = 0.3488
	all data	R1 = 0.1079, wR2 = 0.3635
Weighting scheme	$w=1/[\sigma^2(F_o^2)+(0.2000P)^2]$ where $P=(F_o^2+2F_c^2)/3$	
Largest diff. peak and hole	4.106 and -0.956 $eÅ^{-3}$	
R.M.S. deviation from mean	0.211 $eÅ^{-3}$	

Data for Ho-**hpt**-MOF-1

A total of 1947 frames were collected. The total exposure time was 21.89 hours. The frames were integrated with the Bruker SAINT software package using a narrow-frame algorithm. The integration of the data using a trigonal unit cell yielded a total of 37970 reflections to a maximum θ angle of 44.78° (1.09 Å resolution), of which 6099 were independent (average redundancy 6.226, completeness = 98.4%, R_{int} = 6.79%, R_{sig} = 4.77%) and 4863 (79.73%) were greater than $2\sigma(F^2)$. The final cell constants of a = 39.4817(19) Å, b = 39.4817(19) Å, c = 48.507(3) Å, volume = 65483.(7) $Å^3$, are based upon the refinement of the XYZ-centroids of 9956 reflections above 20 σ(I) with 7.751° < 2θ < 89.47°. Data were corrected for absorption effects using the Multi-Scan method (SADABS). The ratio of minimum to maximum apparent transmission was 0.654. The structure was solved and refined using the Bruker SHELXTL Software Package, using the space group R -3 m, with Z = 6 for the formula unit, $C_{161}H_{75}Ho_9O_{71}S_{12}$. The final anisotropic full-matrix least-squares refinement on $F^2$with 398 variables converged at R1 = 15.13%, for the observed data and wR2 = 45.73% for all data. The goodness-of-fit was 2.069. The largest peak in the final difference electron density synthesis was 3.503 $e^-/Å^3$ and the largest hole was -1.879 $e^-/Å^3$ with an RMS deviation of 0.200 $e^-/Å^3$. On the basis of the final model, the calculated density was 0.763 g/cm^3 and F(000), 14424 e^-. CCDC No.: 2012454.

Table S6. Sample and crystal data for Ho-**hpt**-MOF-1.

Identification code	Ho-**hpt**-MOF-1.	
Chemical formula	$C_{161}H_{75}Ho_9O_{71}S_{12}$	
Formula weight	5014.30 g/mol	
Temperature	200(2) K	
Wavelength	1.54178 Å	
Crystal system	trigonal	
Space group	R -3 m	
Unit cell dimensions	a = 39.4817(19) Å	α = 90°
	b = 39.4817(19) Å	β = 90°
	c = 48.507(3) Å	γ = 120°
Volume	65483.(7) $Å^3$	
Z	6	
Density (calculated)	0.763 g/cm^3	
Absorption coefficient	3.739 mm^{-1}	
F(000)	14424	
Theta range for data collection	3.54 to 44.78°	
Index ranges	-33<=h<=35, -35<=k<=35, -43<=l<=44	
Reflections collected	37970	
Independent reflections	6099 [R(int) = 0.0679]	
Coverage of independent reflections	98.4%	
Absorption correction	Multi-Scan	
Structure solution technique	direct methods	
Structure solution program	SHELXT 2014/5 (Sheldrick, 2014)	
Refinement method	Full-matrix least-squares on F^2	
Refinement program	SHELXL-2018/3 (Sheldrick, 2018)	
Function minimized	$\Sigma w(F_o^2 - F_c^2)^2$	
Data / restraints / parameters	6099 / 1 / 398	

Goodness-of-fit on F^2	2.069	
Δ/σ_{max}	0.180	
Final R indices	4863 data; I>2σ(I)	R1 = 0.1513, wR2 = 0.4235
	all data	R1 = 0.1752, wR2 = 0.4573
Weighting scheme	$w=1/[\sigma^2(F_o^2)+(0.2000P)^2]$ where $P=(F_o^2+2F_c^2)/3$	
Largest diff. peak and hole	3.503 and -1.879 eÅ^{-3}	
R.M.S. deviation from mean	0.200 eÅ^{-3}	

Data for Y-**ken**-MOF-1

A specimen of C106 H64 O36 Y9 was used for the X-ray crystallographic analysis. The X-ray intensity data were measured (λ = 1.54178 Å). The total exposure time was 9.90 hours. The frames were integrated with the Bruker SAINT software package using a narrow-frame algorithm. The integration of the data using a trigonal unit cell yielded a total of 172887 reflections to a maximum θ angle of 44.59° (1.10 Å resolution), of which 9775 were independent (completeness = 99.6%, R_{int} = 3.66%). The final cell constants of a = 25.4495(5) Å, b = 25.4495(5) Å, c = 39.5438(8) Å, volume = 22180.3(10) Å^3, are based upon the refinement of the XYZ-centroids of 9891 reflections above 20 σ(I) with 7.297° < 2θ < 88.84°. Data were corrected for absorption effects using the Multi-Scan method (SADABS). The ratio of minimum to maximum apparent transmission was 0.935.

The nonanuclear $[Y_9(\mu_3\text{-}O)_2(\mu_3\text{-}OH)_{12}(OH)_2(H_2O)_{11}]^{8+}$ cluster is statistically disorder over two positions which impose disorder also on the organic linker (see Figure S13 below). In particular, the six lateral ligands are 2-fold disordered while the axial ligands are 3-fold. Regarding the Y_9-cluster, the “upper” and “lower” Y-triangles were modelled with a 2-fold disorder however, the "middle" Y-triangle is not assigned to PARTs as all of its positions of both triangles are symmetry generated from one position (Figure S13). For this reason, the occupancy for this atom was set to 0.5 to fully describe the disorder.

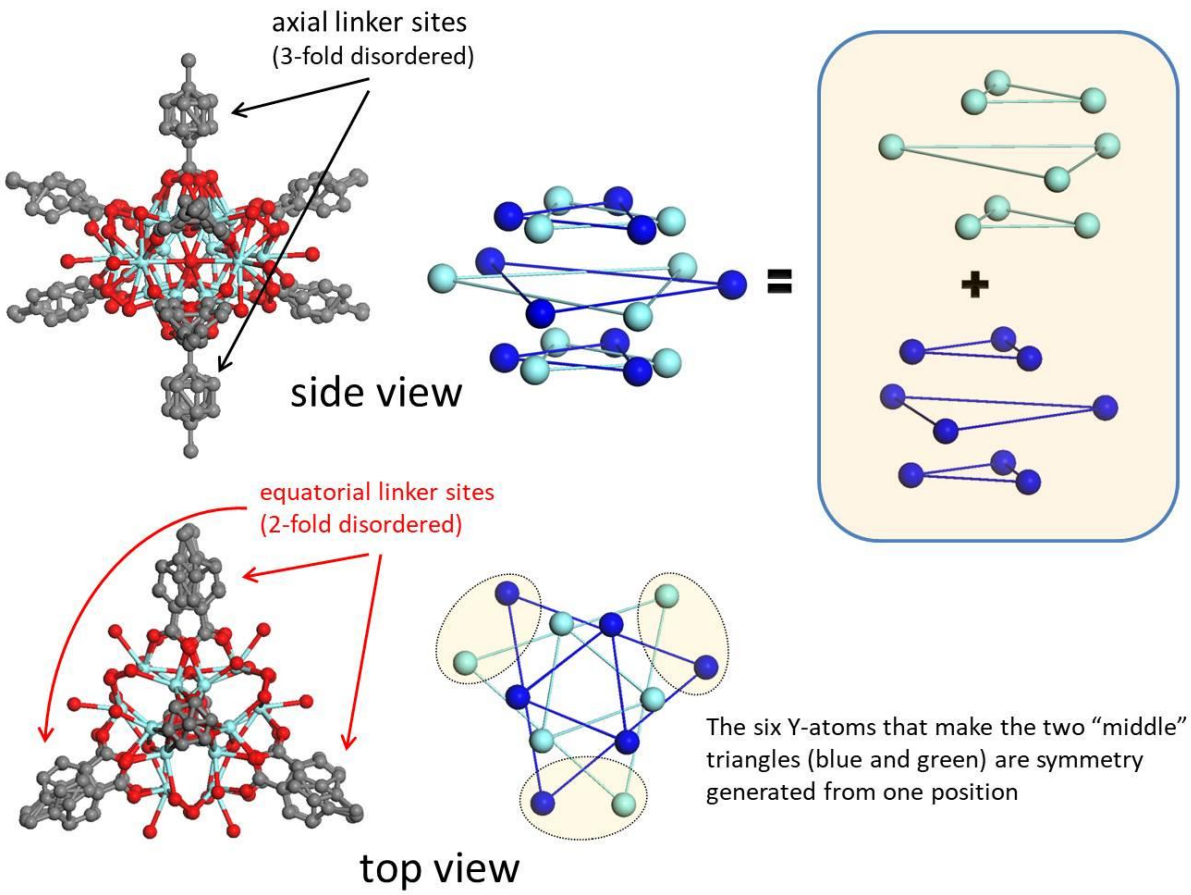

Figure S12. Structural disorder observed in Y-**ken**-MOF-1.

In addition to the observed disorder, merohedral twinning is also involved and included in the refinement. The final full-matrix least-squares refinement on F^2 with 427 variables converged at R1 = 13.57%, for the observed data and wR2 = 36.62% for all data, after running SQUEEZE routine. The goodness-of-fit was 4.560. The largest peak in the final difference electron density synthesis was 1.348 $e^-/Å^3$ and the largest hole was –0.539 $e^-/Å^3$. The crystal and refinement data are summarized in Table 11. CCDC No.: 2012456.

Table S7. Crystal data and structure refinement for Y-**ken**-MOF-1.

Empirical formula	C106 H64 O36 Y9
Formula weight	2713.76
Temperature	200(2) K
Wavelength	1.54178 Å
Crystal system	trigonal
Space group	P -3 1 c
Unit cell dimensions	a = 25.4495(5) Å, α = 90° b = 25.4495(5) Å, β = 90° c = 39.5438(8) Å, γ = 120°
Volume	22180.3(10) $Å^3$
Z	2
Density (calculated)	0.406 g/cm^3

Absorption coefficient	1.670 mm^{-1}
F(000)	2678
Crystal size	0.06 x 0.03 x 0.03 mm^3
θ range for data collection	2.004 to 56.408°
Index ranges	-27<=h<=27, -23<=k<=27, -41<=l<=42
Reflections collected	172887
Independent reflections	9775 [R_{int} = 0.0366]
Completeness to θ = 56.408°	99.8%
Refinement method	Full-matrix least-squares on F^2
Data / restraints / parameters	9775 / 963 / 427
Goodness-of-fit	4.560
Final R indices [I > 2σ(I)]	R_{obs} = 0.1357, wR_{obs} = 0.3662
R indices [all data]	R_{all} = 0.1682, wR_{all} = 0.3768
Extinction coefficient	.
Largest diff. peak and hole	1.348 and -0.539 e·$Å^{-3}$

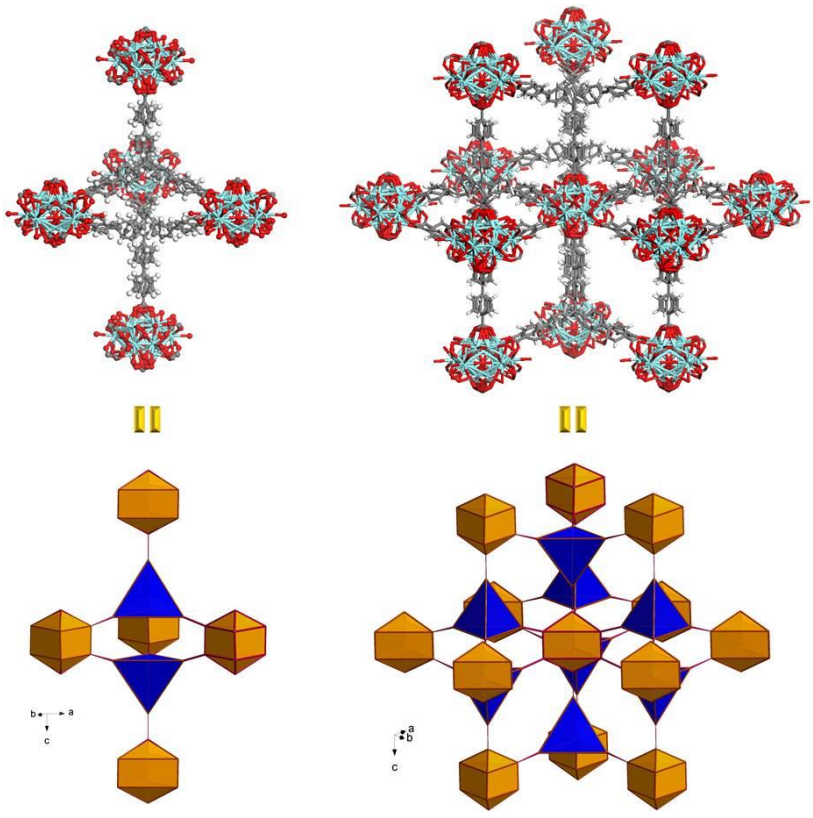

Figure S13. Along the c-axis in Y-**ken**-MOF-1, pairs of opposite linkers are formed and connect six Y_9-clusters in a regular trigonal prismatic arrangement (left). Each Y_9-cluster is connected to twelve other Y_9-clusters, six in equatorial position via three pairs of linkers and six more, three on the top and three on the bottom, via two more linkers (right).

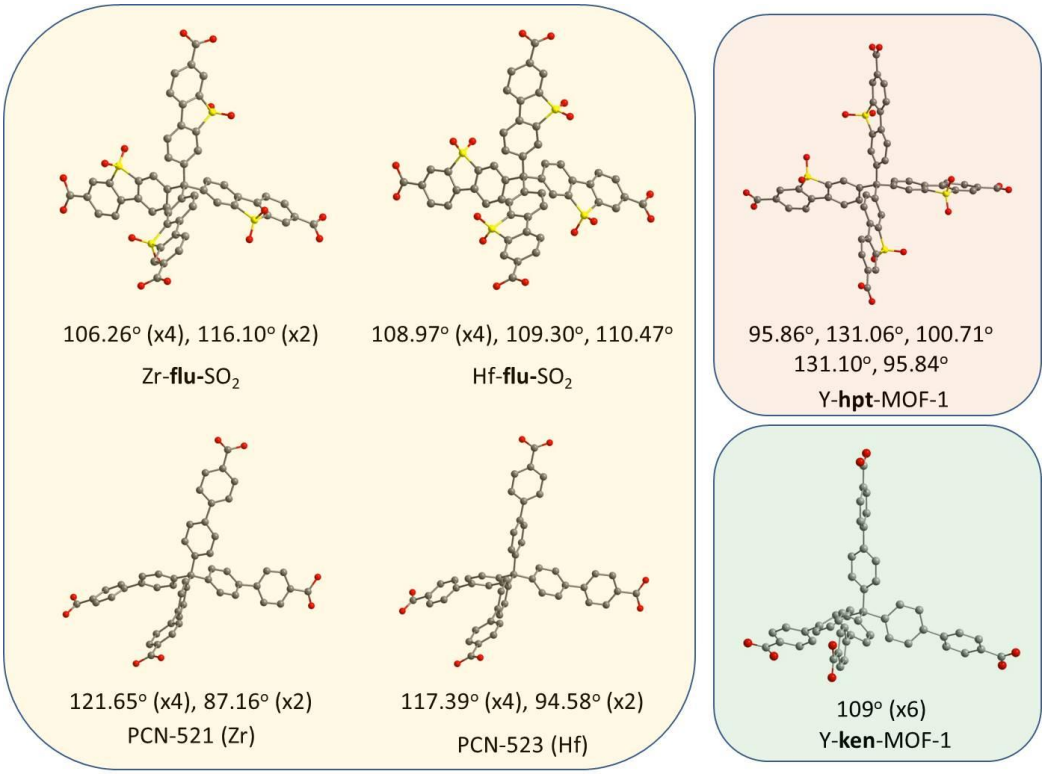

Figure S14. Ligand conformation in the indicated MOFs, as revealed by SCXRD.

Powder X-ray diffraction measurements

The phase purity and stability in different solvents of M-**flu**-SO_2 (M: Zr, Hf) was verified using powder X-ray diffraction (PXRD) analysis.

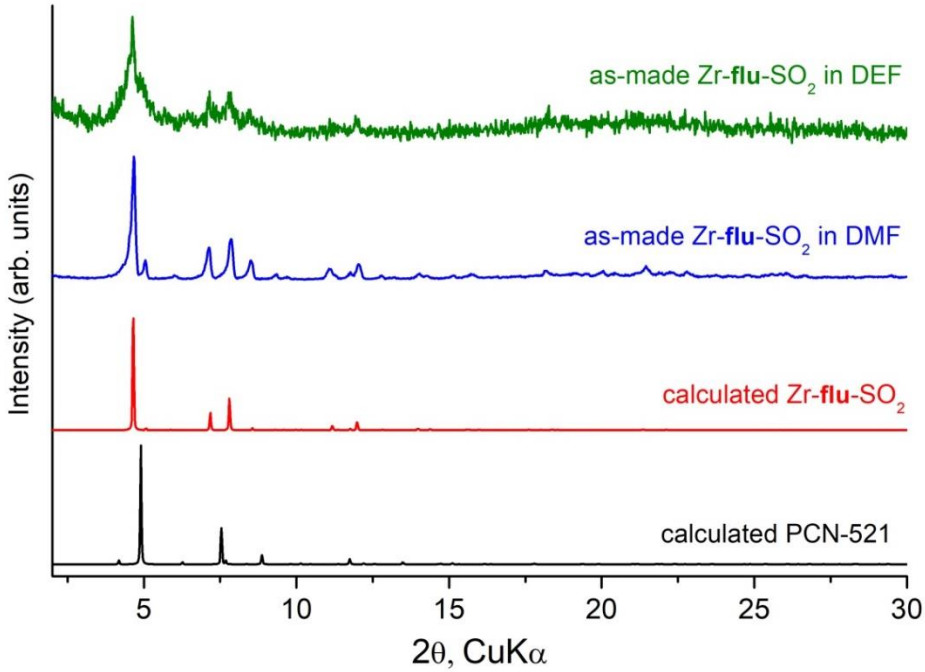

Figure S15. Experimental PXRD pattern of as-made Zr-**flu**-SO_2 synthesized in DMF (blue) and DEF (green), along with the calculated pattern from the corresponding single crystal structure of Zr-**flu**-SO_2 (red) and PCN-521 (black).

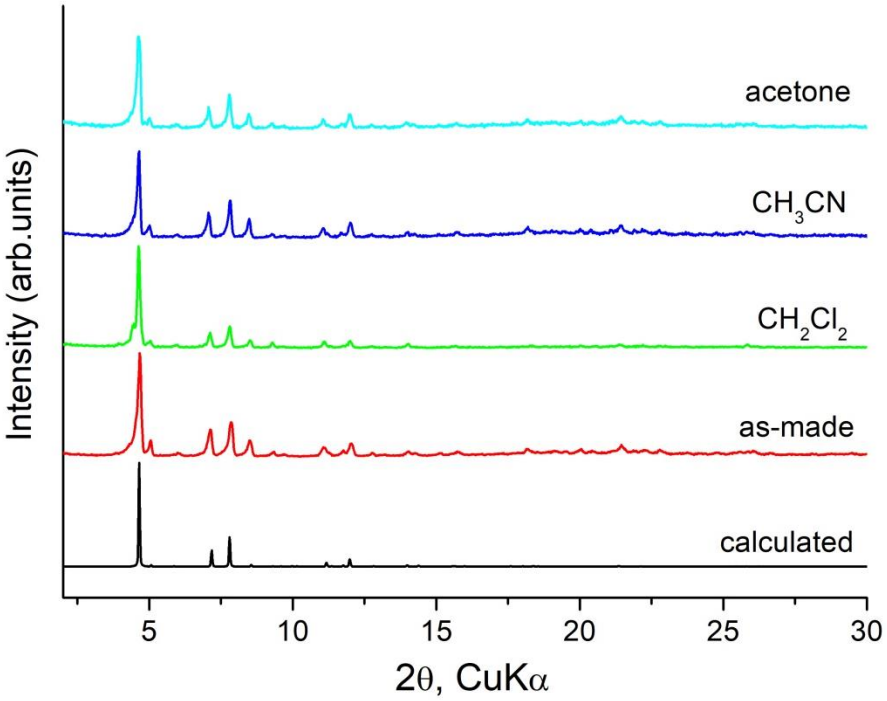

Figure S16. Experimental PXRD pattern of as-made Zr-**flu**-SO_2 (red), along with the calculated pattern from the corresponding single crystal structure (black). PXRD pattern of Zr-**flu**-SO_2 after exchange with dichloromethane (green), acetonitrile (dark blue) and acetone (light blue).

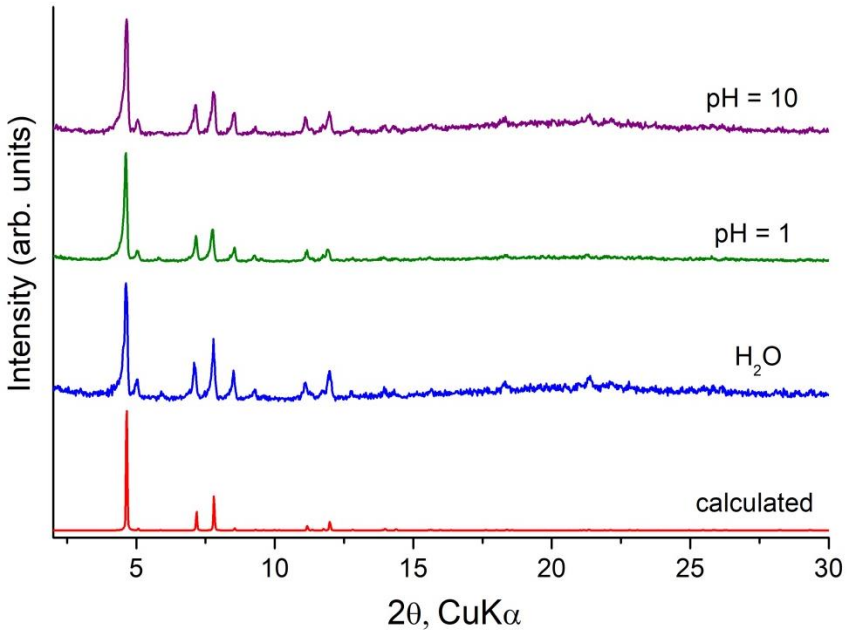

Figure S17. Experimental PXRD pattern of Zr-**flu**-SO_2 treated with H_2O (blue), in pH 1 (green) and in pH 10 (purple), along with the corresponding calculated pattern from the single crystal structure (red).

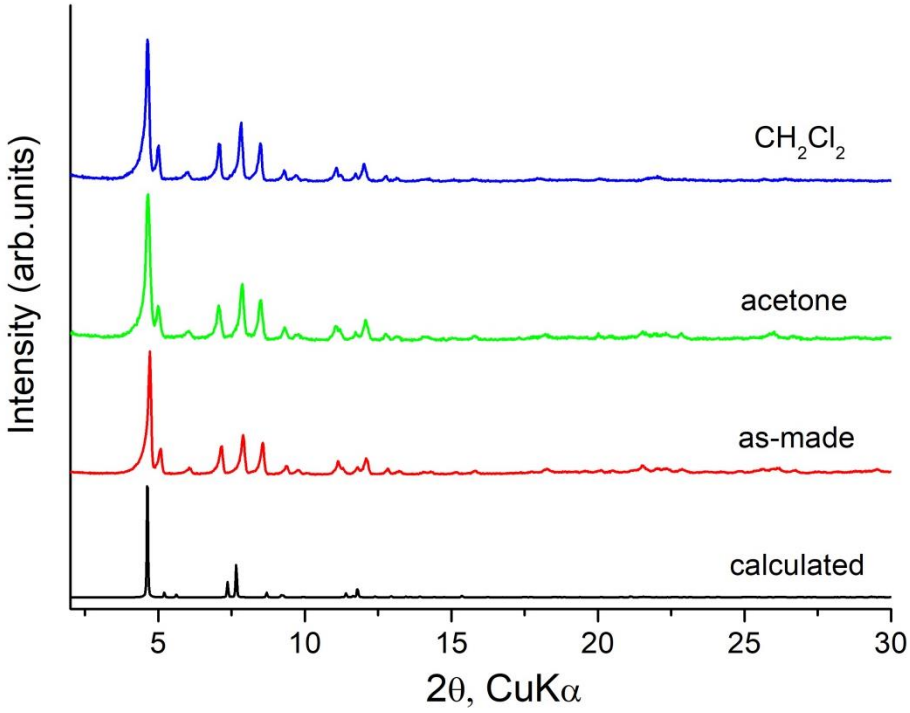

Figure S18. Experimental PXRD pattern of as-made Hf-**flu**-SO_2 (red), along with the calculated pattern from the corresponding single crystal structure (black). PXRD pattern of Hf-**flu**-SO_2 after exchange with dichloromethane (green), acetonitrile (dark blue) and acetone (light blue).

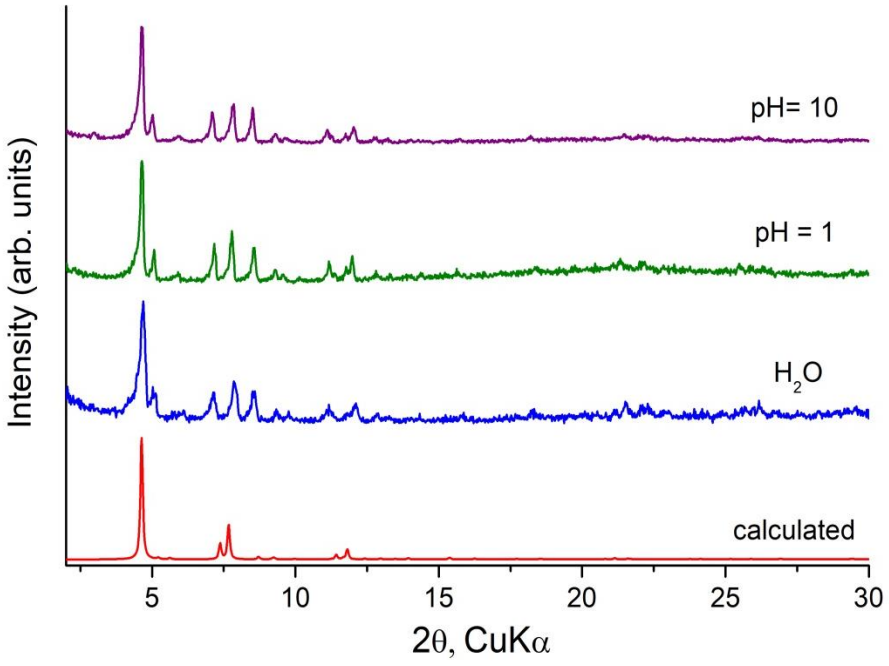

Figure S19. Experimental PXRD pattern of Hf-**flu**-SO_2 treated with H_2O (blue), in pH 1 (green) and in pH 10 (purple), along with the corresponding calculated pattern from the single crystal structure (red).

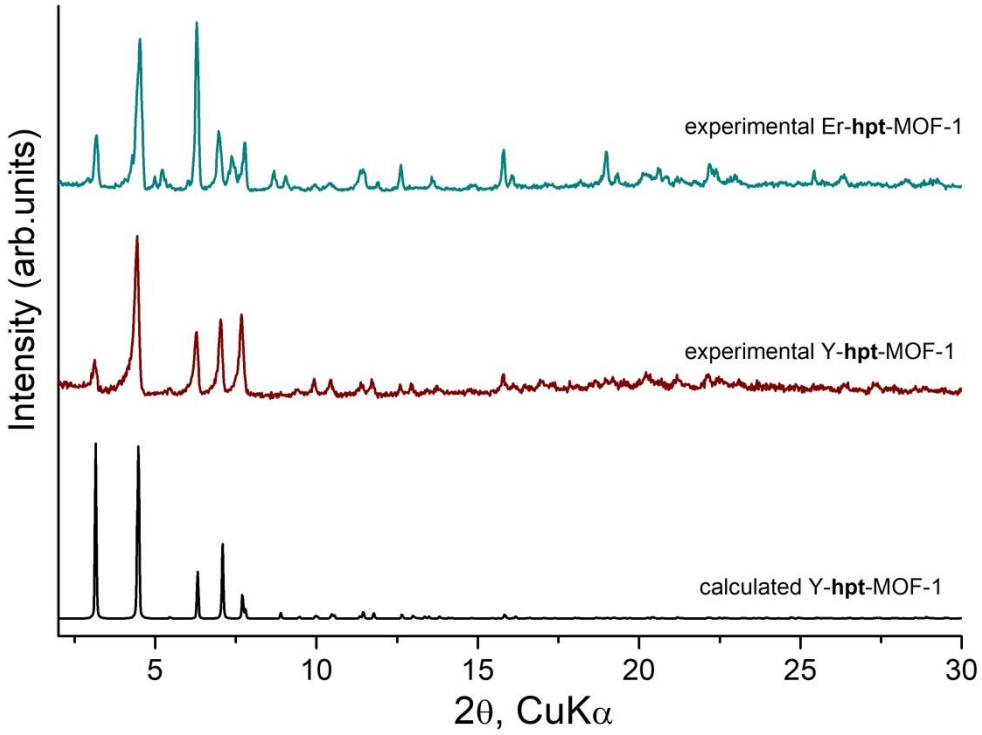

Figure S20. Experimental PXRD pattern of as-made Y-**hpt**-MOF-1 and Er-**hpt**-MOF-1 along with the calculated pattern from the single crystal structure of Y-**hpt**-MOF-1.

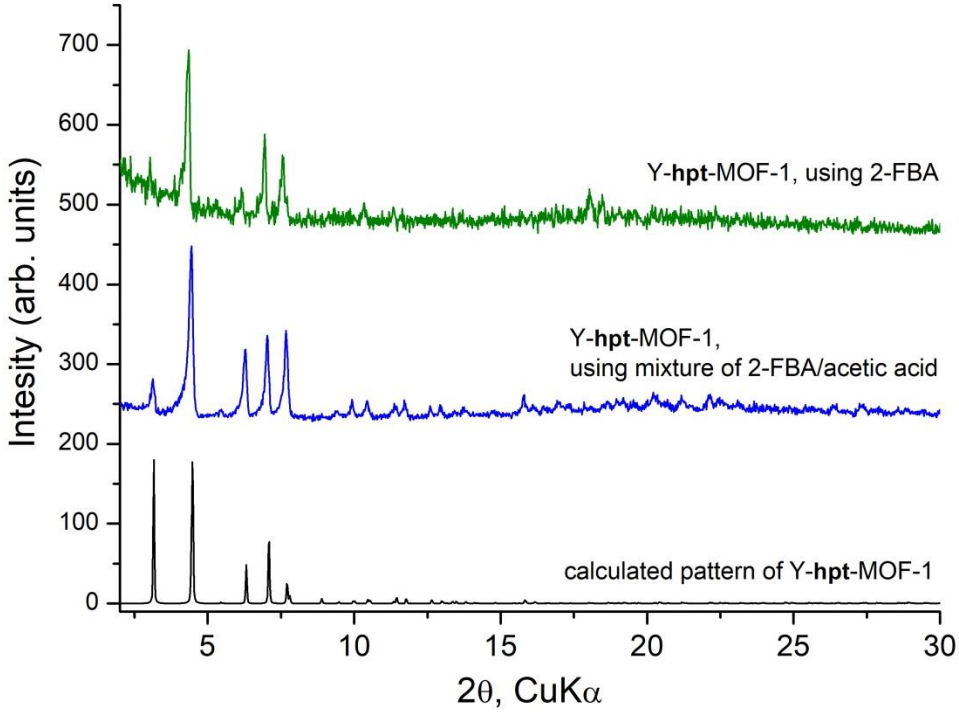

Figure S21. Experimental PXRD pattern of Y-**hpt**-MOF-1 synthesized using only 2-FBA as modulator (green line) along with the pattern obtained from the solid synthesized in a mixture of 2FBA/acetic acid (blue line) and the calculated pattern from the single crystal structure (black line).

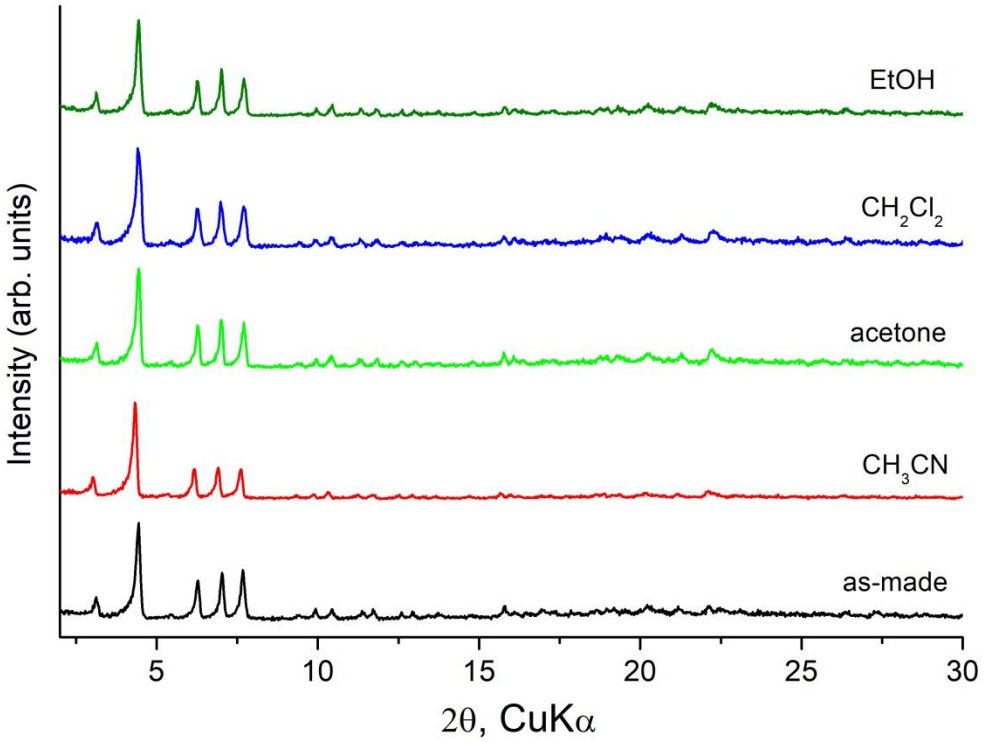

Figure S22. PXRD pattern of Y-**hpt**-MOF-1 after exchange with different solvents.

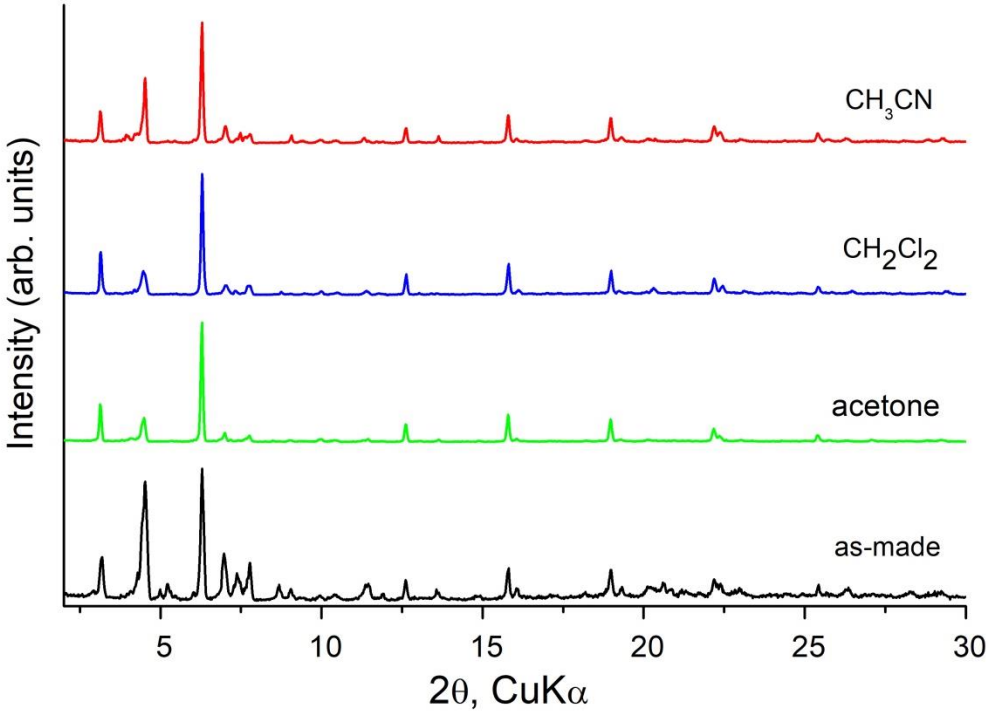

Figure S23. PXRD pattern of Er-**hpt**-MOF-1 after exchange with different solvents.

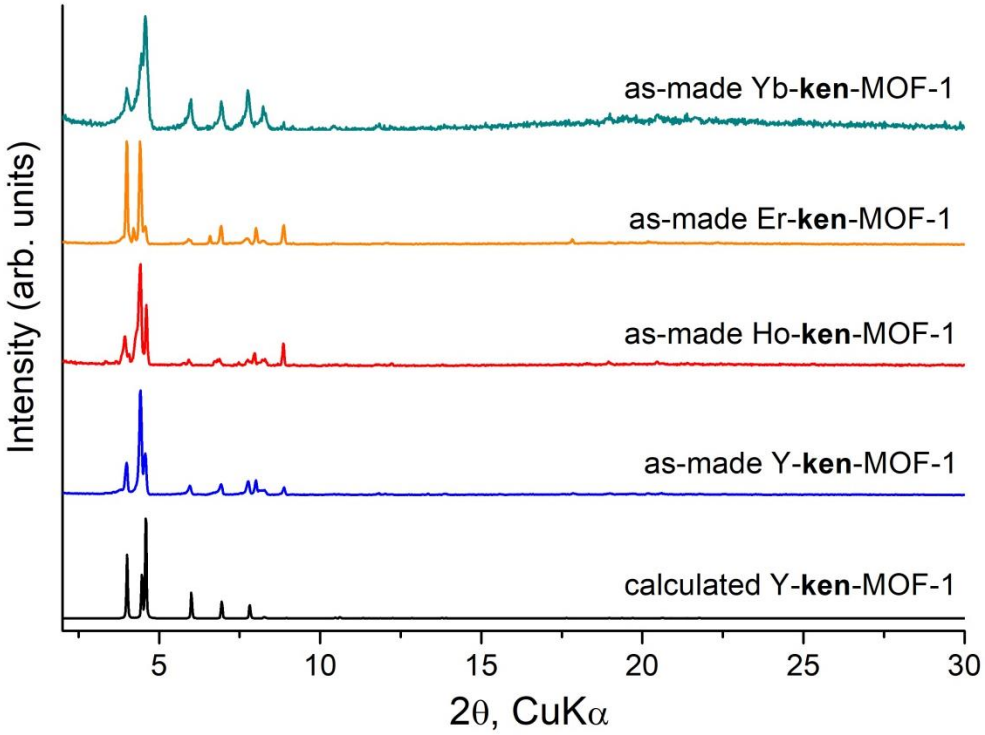

Figure S24. Experimental PXRD pattern of the as-made RE-**ken**-MOF-1 solids (RE: Y^{3+}, Ho^{3+}, Er^{3+}, Yb^{3+}) along with the calculated pattern from the single crystal structure of Y-**ken**-MOF-1.

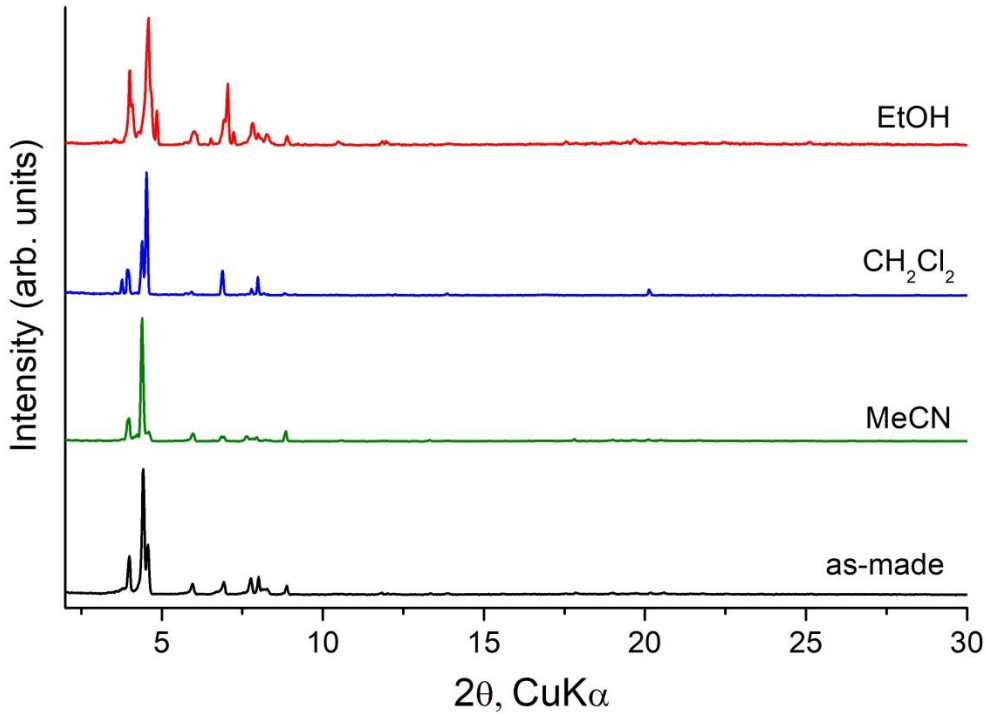

Figure S25. PXRD pattern of Y-**ken**-MOF-1 after exchange with different solvents.

Energy Dispersive Spectroscopy (EDS)

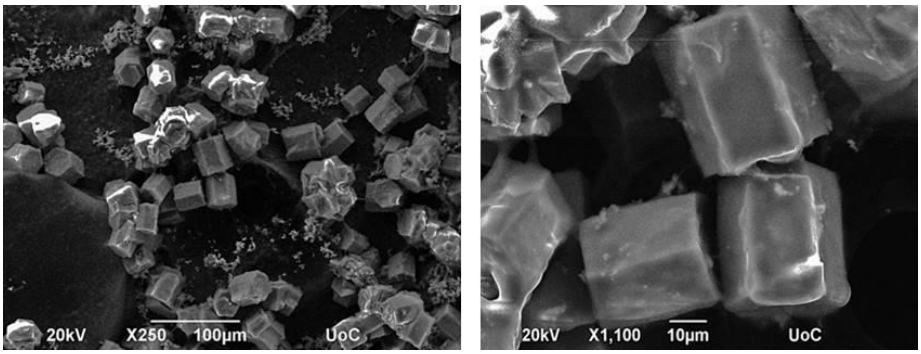

Figure S26. SEM images of a $NaNO_3$ treated Yb-**ken**-MOF-1.

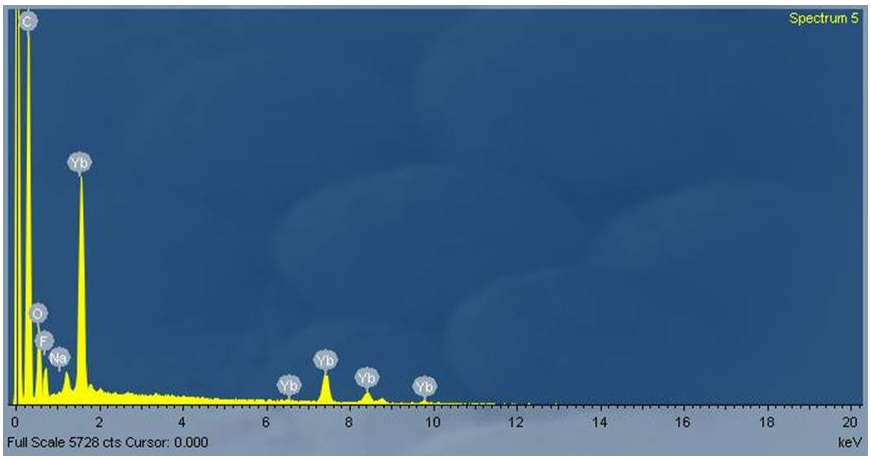

Figure S27. EDS spectrum of $NaNO_3$ treated Yb-**ken**-MOF-1.

Table S8. EDS quantitative analysis results for Yb-**ken**-MOF-1.

Element	Atomic%
C K	74.30
O K	17.77
F K	6.42
Na K	**-0.02**
Yb L	**1.53**

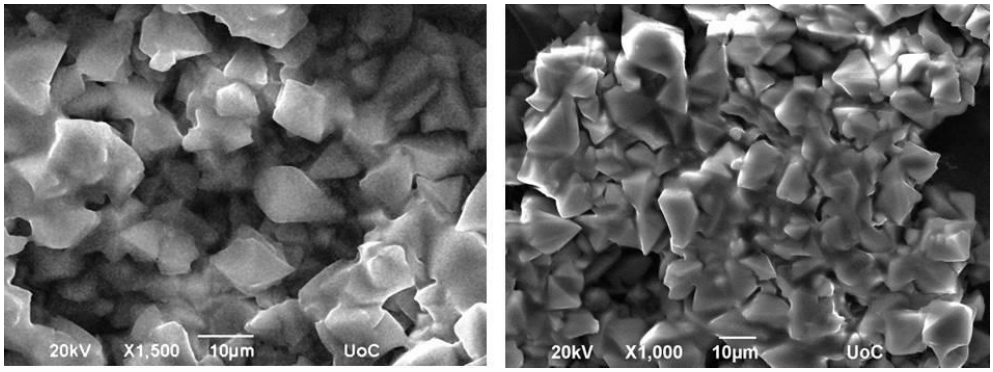

Figure S28. SEM images of $NaNO_3$ treated Er-**hpt**-MOF-1.

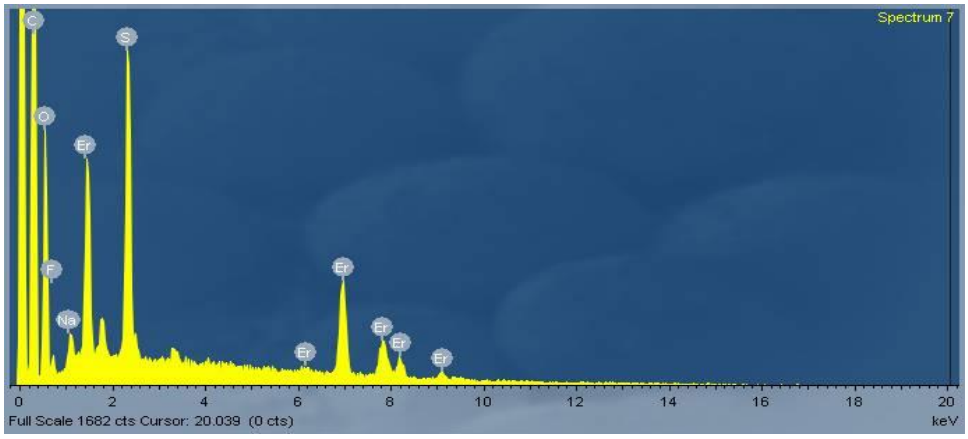

Figure S29. EDS spectrum of $NaNO_3$ treated Er-**hpt**-MOF-1.

Table S9. EDS quantitative analysis results for Er-**hpt**-MOF-1.

Element	Atomic%
C K	71.31
O K	22.91
F K	1.43
Na K	**0.40**
S K	**2.68**
Er L	**1.26**

Gas sorption measurements and analysis

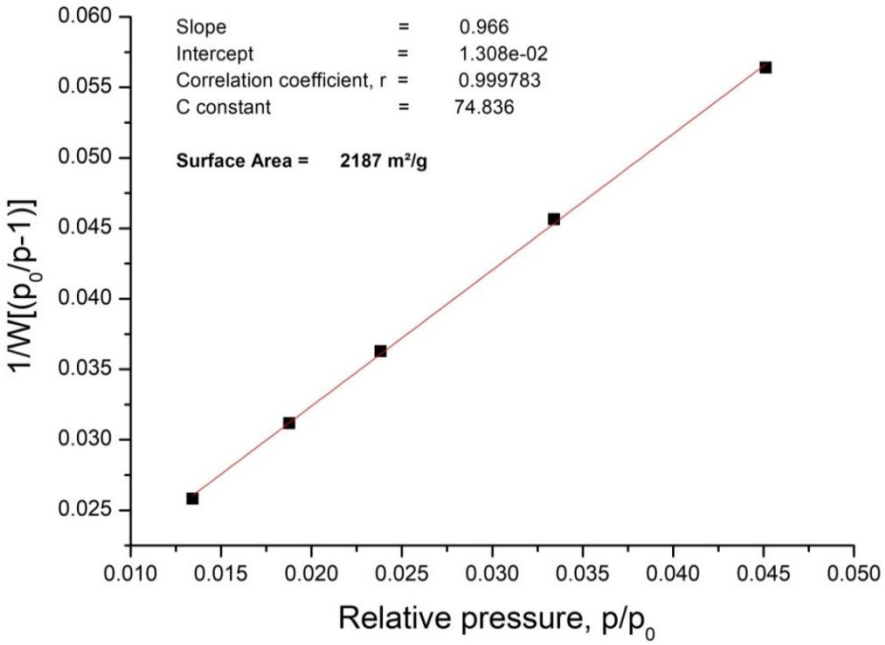

Figure S30. BET plot for Zr-**flu**-SO_2 calculated from the corresponding Ar adsorption isotherm at 87 K.

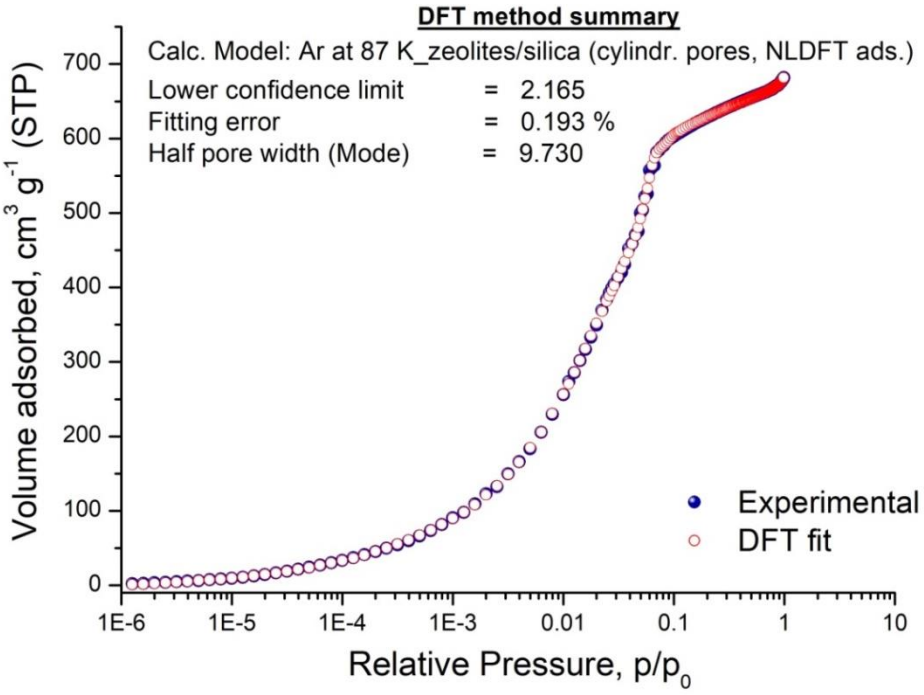

Figure S31. Argon adsorption isotherm of Zr-**flu**-SO_2 at 87 K in logarithmic scale and the corresponding NLDFT fitting.

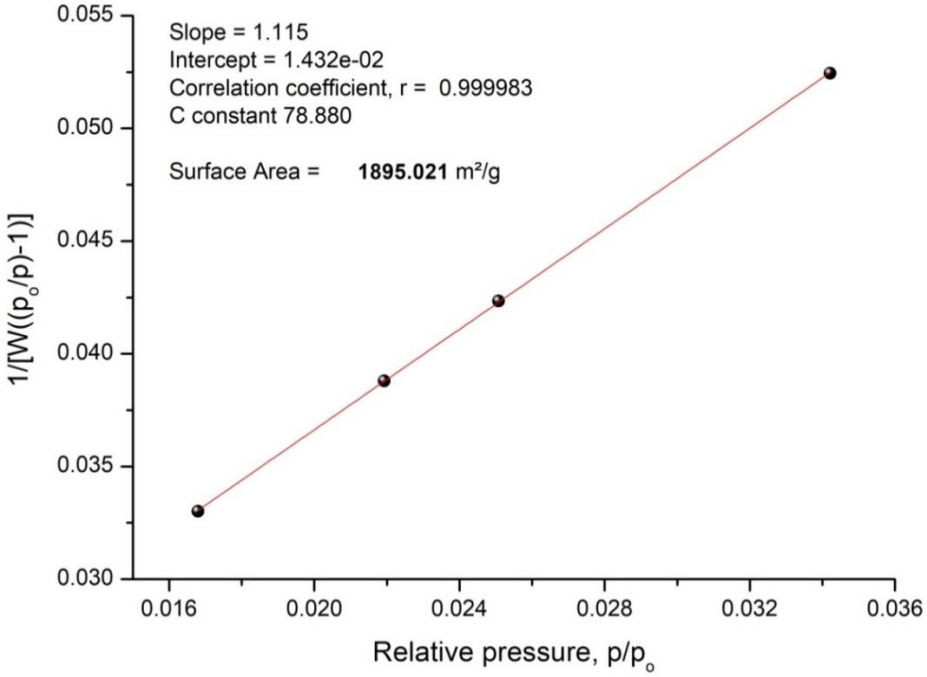

Figure S32. BET plot for Hf-**flu**-SO_2 calculated from the corresponding Ar adsorption isotherm at 87K.

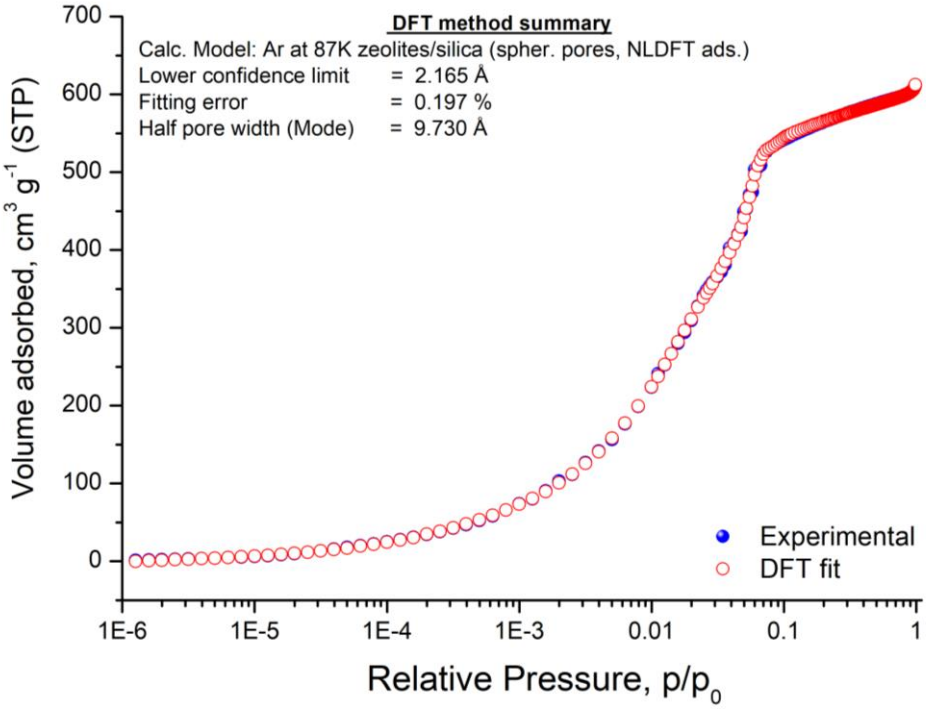

Figure S33. Argon adsorption isotherm of Hf-**flu**-SO_2 at 87 K in logarithmic scale and the corresponding NLDFT fitting.

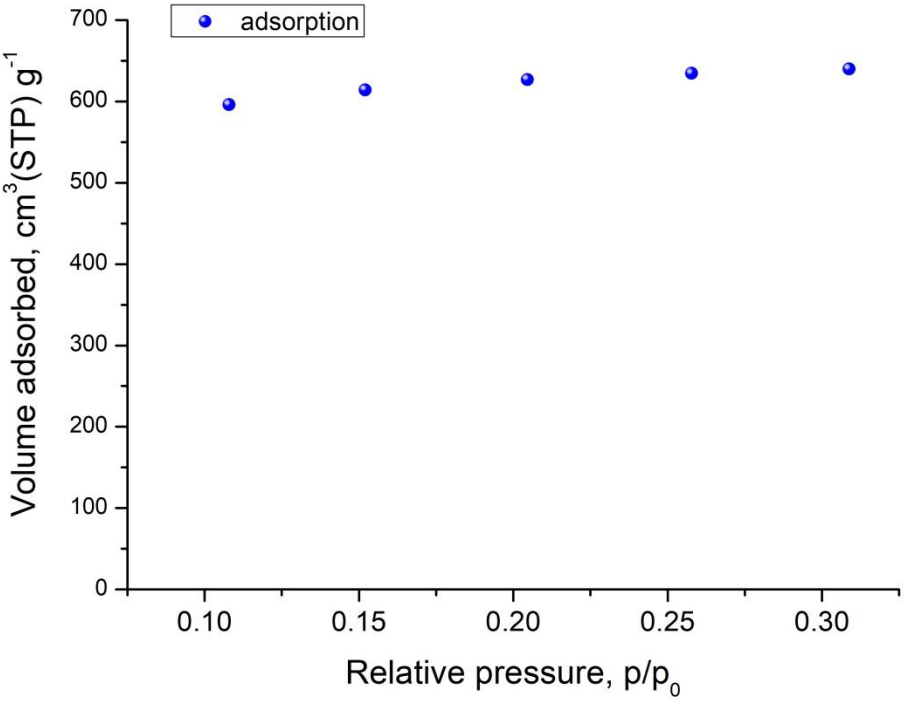

Figure S34. Five point N_2 isotherm of PCN-521 recorded at 77 K.

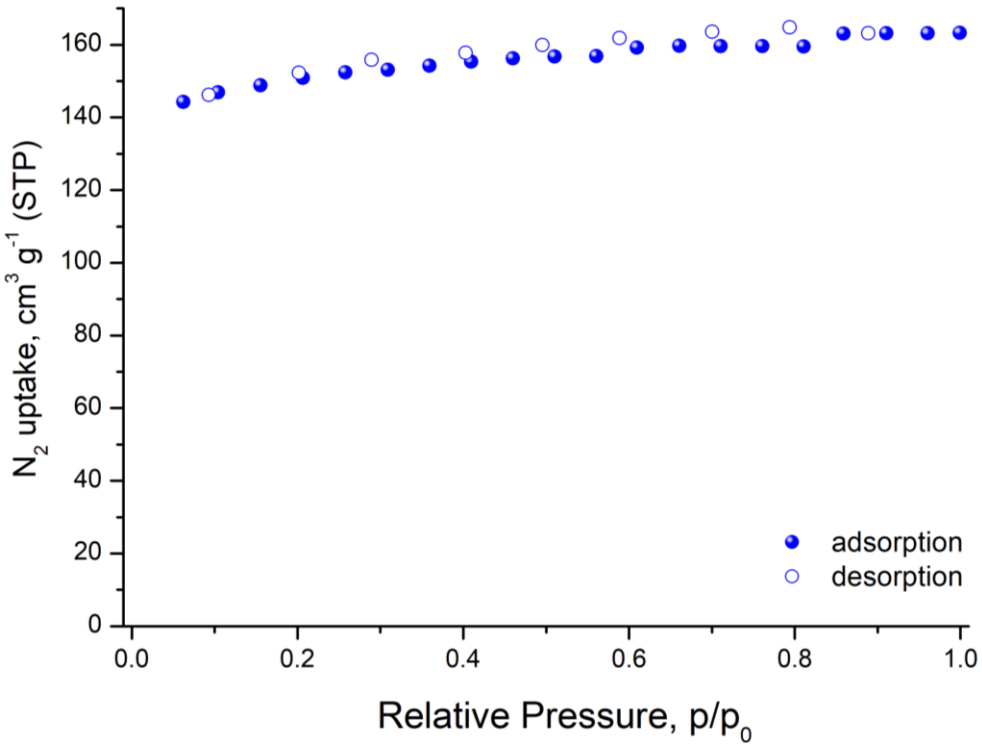

Figure S35. Nitrogen sorption isotherm of the Y-**hpt**-MOF-1 recorded at 77 K.

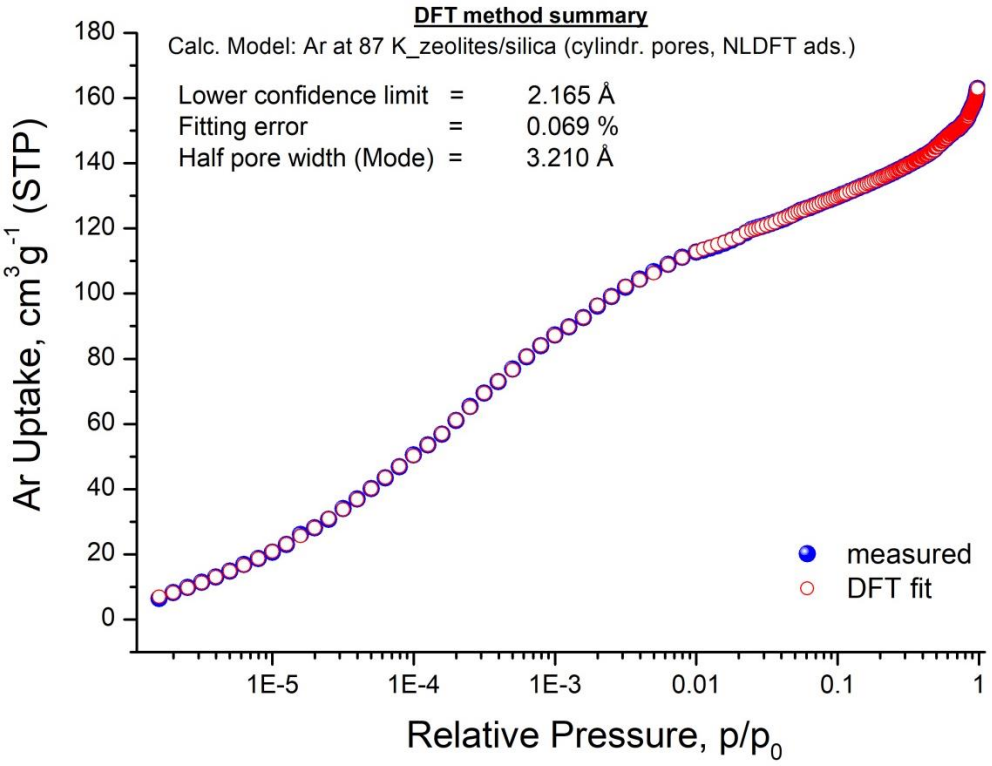

Figure S36. Argon sorption isotherm of the Y-**hpt**-MOF-1 recorded at 87 K in logarithmic scale and the corresponding NLDFT fitting.

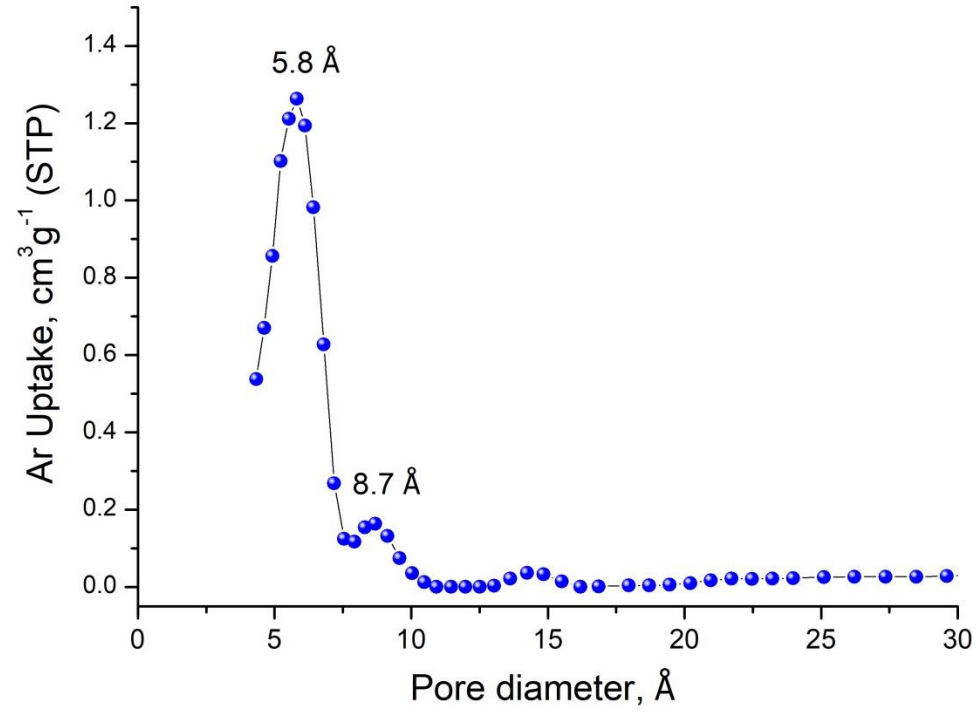

Figure S37. Pore size distribution obtained by NLDFT method for Y-**hpt**-MOF-1.

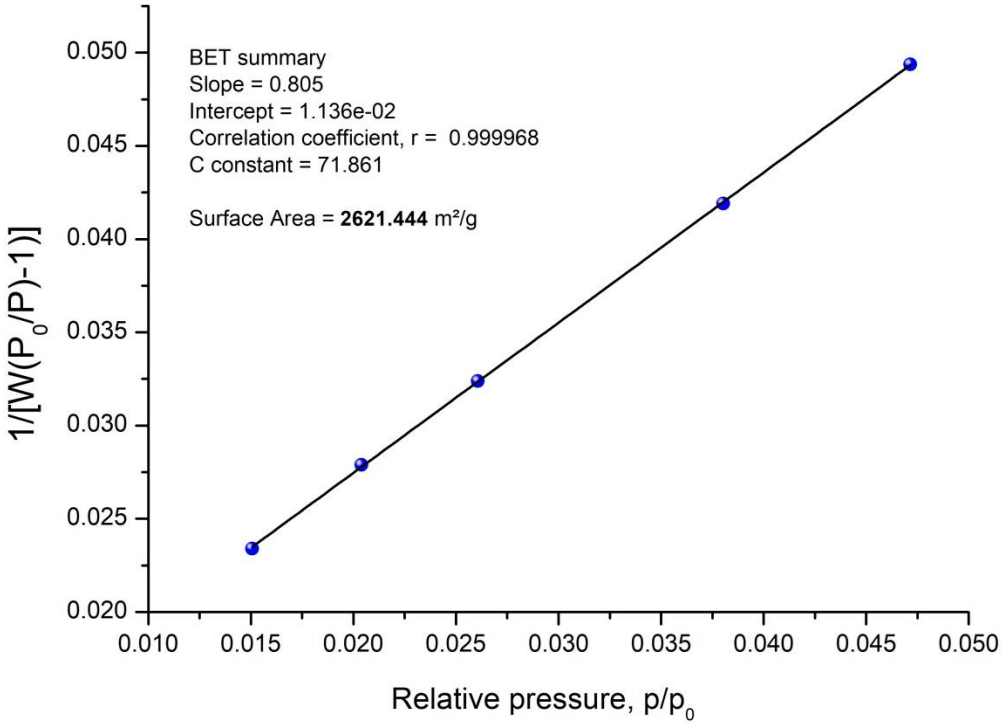

Figure S38. BET plot for Y-**ken**-MOF-1 from the Ar adsorption isotherm at 87 K.

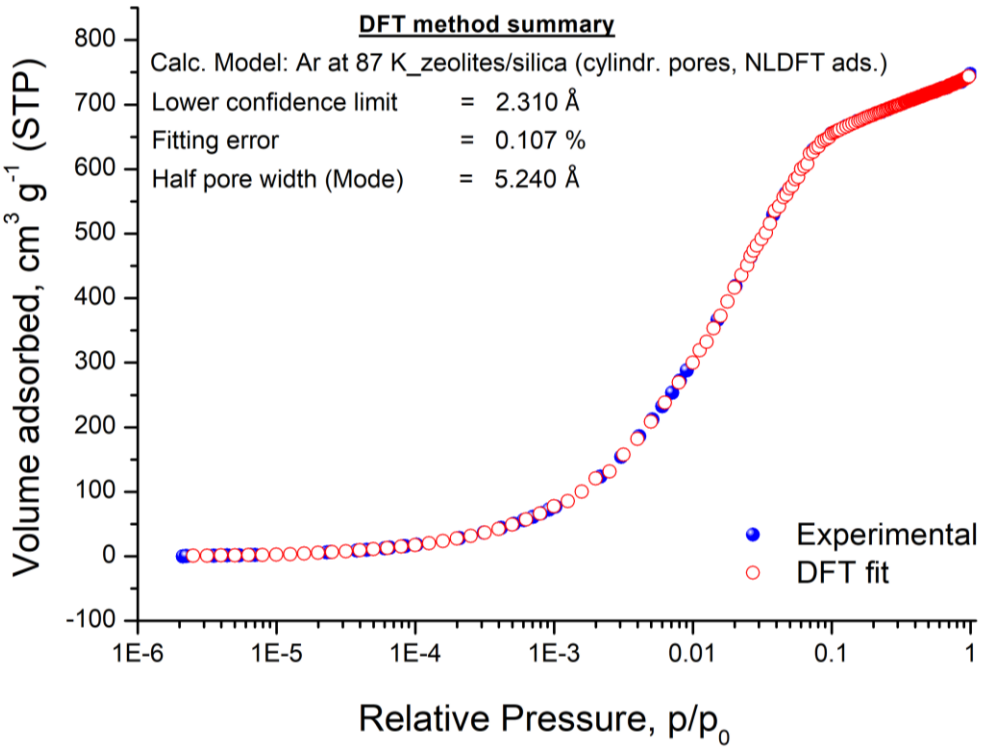

Figure S39. Argon adsorption isotherm of Y-**ken**-MOF-1 at 87K in logarithmic scale and the corresponding NLDFT fitting.

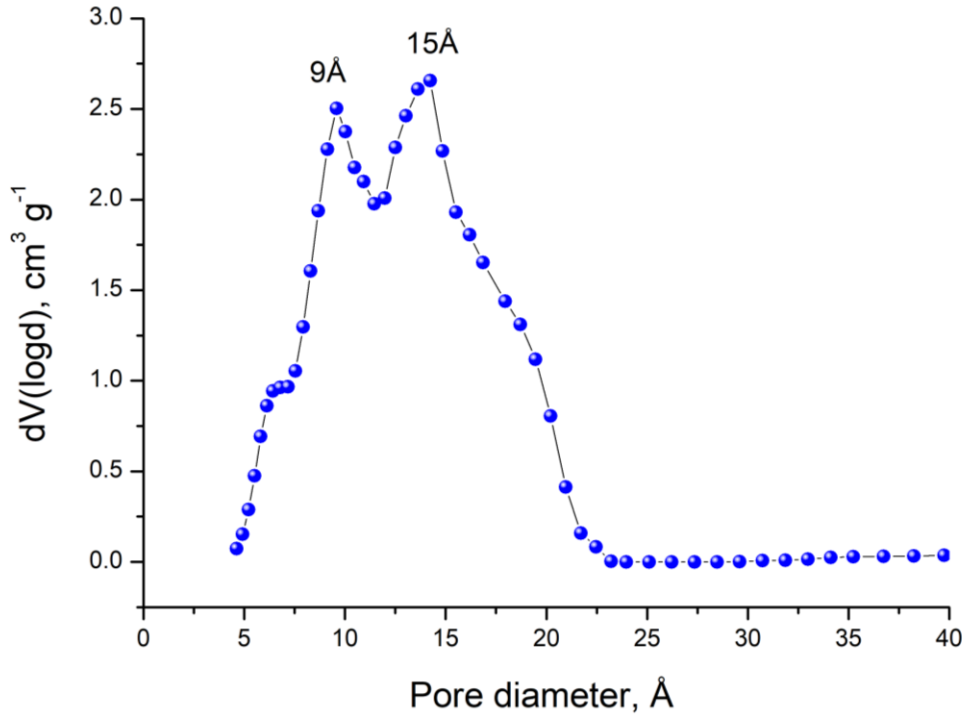

Figure S40. Pore size distribution obtained by NLDFT method for Y-**ken**-MOF-1.

Table S10. Porosity data of representative highly porous RE-based MOFs.

Material	Gas uptake ($cm^3 g^{-1}$)	BET area ($m^2 g^{-1}$)	Exp. total pore volume ($cm^3 g^{-1}$)	Calc. total pore volume ($cm^3 g^{-1}$)	Reference
Y-**ftw**-MOF-2	1000[c]	3690	1.26	1.26	37
Y-**ftw**-MOF(Napth)	800[c]	3040	1.05	1.11	37
Y-**ken**-MOF-1	747	**2621**	0.95	1.86	This work
Y-FTZBP	750	2410	0.94	1.03	31
Y-**shp**-MOF-1	620	2200	0.79	0.9	34
Y-**ftw**-MOF-2 (Anthr)	600[c]	2100	0.79	1.05	37
Eu-SPFF[b]	514	1891	0.79		S[3]
Tb-**urx**-MOF-1	500	1590	0.66	0.82	33
Y-**kex**-MOF-1[b]	542	1580	0.84	1.23	33
Y-**shp**-MOF-5	450[c]	1550	0.63	0.61	35
Y-**gea**-MOF-1	450[c]	1490	0.58	0.71	S[4]
Y-**pek**-MOF-1	460[c]	1330	0.47	0.47	36
Y-**aea**-MOF	360[c]	-	-	-	36
Y-**alb**-MOF-1	360	-	0.52	0.63	34
Yb-DPPY[b]	200[c]	1226	0.49	0.57	S[5]
PCN-905-SO_2-BDC [b]	330	916	-	-	20
Y-csq-MOF-1	296	874	0.37	0.63	41
PCN-906-O[b]	250	830	-	-	20
PCN-912(Eu)-CH_3(50%)[b]	292	829	0.55	0.68	24
Tb-UTSA-61[b]	450	770	0.67	1.66	S[6]
Yb-DDIA[b]	300[c]	759	0.3	0.49	S[5]
Y-**kce**-MOF-1[b]	244	720	0.37	1.42	33
PCN-918(Eu) [b]	225	673	0.38	0.49	24
PCN-918(Tb) [b]	221	670	0.36	-	24
PCN-909(Eu)-Cl[b]	232	661	0.54	0.88	24
PCN-905-SO_2 [b]	216	633	-	-	20
PCN-909(Tb)-NH_2[b]	220	608	0.5	0.57	24
PCN-918(Tb)-OCH_3[b]	208	602	0.33	-	24
Y-**hpt**-MOF[b]	163	526	0.24	1.12	This work

[a] Ar sorption isotherm at 87 K. [b] N_2 sorption isotherm at 77 K. [c] Estimated from the reported isotherm.

Low pressure CO_2, CH_4 and Xe sorption isotherms, determination of heat of adsorption and CO_2/CH_4 selectivity calculations using IAST.

Heat of adsorption. To calculate heats of adsorptions, the corresponding adsorption isotherms at two or three different temperatures were simultaneously fitted using the virial type[7, 8] Equation 1:

$$\ln P = \ln N + \frac{1}{T}\sum_{i=0}^{m} a_i N^i + \sum_{i=0}^{n} b_i N^i \qquad (1)$$

The heat of adsorption at zero coverage was calculated from Equation 2, where as a function of surface coverage, from Equation 3:

$$Q_{st} = -Ra_o \qquad (2)$$

$$Q_{st}(N) = -R\sum_{i=0}^{m} a_i N^i \qquad (3)$$

For the determination of the isosteric heat of adsorption using the Clausious Clapeyron equation a commercially available software, ASiQwin (version 3.01) purchased from Quantachrome, was used.

Gas Selectivity using the IAST model. The corresponding calculations were performed according to an established procedure.[9-11] Specifically, the single-component adsorption isotherms were described by fitting the data with the following virial-type equation

$$p = \frac{n}{K}\exp(c_1 1n + c_2 n^2 + c_3 n^3 + c_4 n^4) \qquad (4)$$

where p is the pressure in Torr, n is the adsorbed amount in mmol g^{-1}, K is the Henry constant in mmol g^{-1} $Torr^{-1}$ and c_i are the constants of the virial equation.

The free energy of desorption at a given temperature and pressure of the gas is obtained from the analytical integration of eq. (4):

$$G(T,p) = RT\int_0^p \frac{n}{p}dp = RT(n + \frac{1}{2}c_1 n^2 + \frac{2}{3}c_2 n^3 + \frac{3}{4}c_3 n^4 + \frac{4}{5}c_4 n^5) \quad (5)$$

The free energy of desorption is a function of temperature and pressure *G(T,p)* and describes the minimum work (Gibbs free energy) that required to completely degas the adsorbent surface.

For a binary mixture of component *i* and *j* eq. (5) yields the individual pure loadings $n_i^0$and n_j^0 at the same free energy of desorption:

$$G_i^0\left(n_i^0\right) = G_j^0(n_j^0) \qquad (6)$$

The partial pressure of component *i* and *j* in an ideal adsorption mixture is given by the following equations:

$$py_i = p_i^0(n_i^0)x_i \qquad (7)$$
$$py_j = p_j^0(n_j^0)x_j \qquad (8)$$

where y_i *(=1-y_j)* and x_i *(=1-x_j)* is the molar fraction of component *i* in the gas phase and the adsorbed phase respectively and p_i^0, $p_j^0$is the pure component pressure of *i* and *j* respectively. From eq. (6)-(8) and (3), the selectivity for the adsorbates *i* and *j* ($S_{i,j}$) and the total pressure (p) of the gas mixture were calculated from eq. (9) and eq. (10), respectively.

$$S_{ij} = \frac{x_i/y_i}{x_j/y_j} = \frac{p_j^0}{p_i^o} \qquad (9)$$
$$p = \sum_i^j (p_i^o\, x_i) \qquad (10)$$

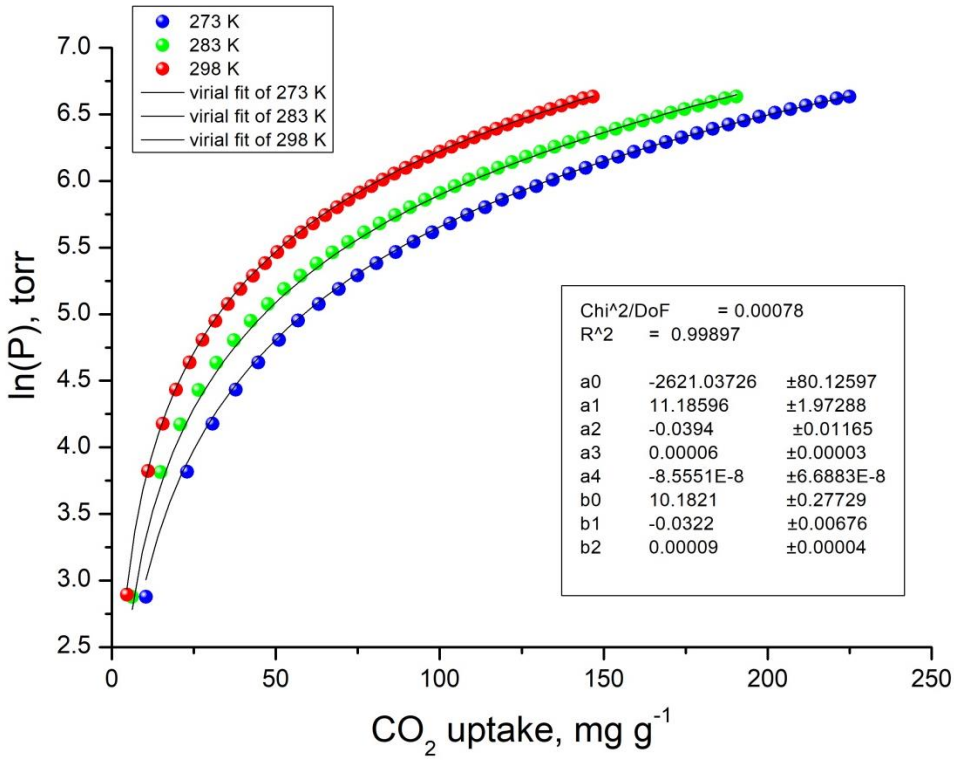

Figure S41. Virial type fitting of CO_2 adsorption isotherms of Zr-**flu**-SO_2 at 273 K, 283 K and 298 K according to equation 1.

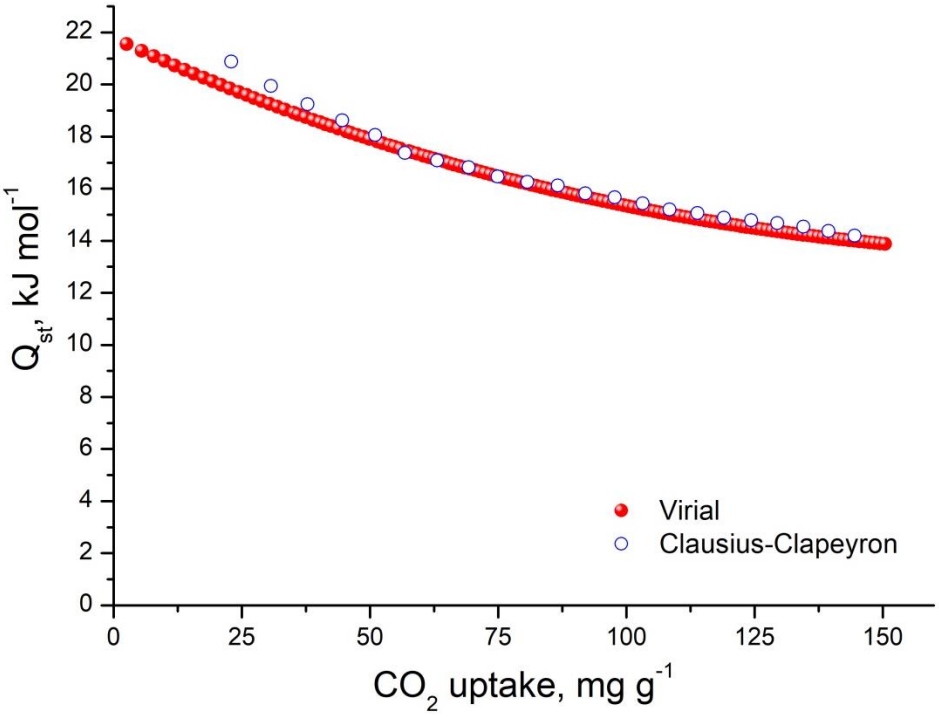

Figure S42. CO_2 isosteric heat of adsorption of Zr-**flu**-SO_2 as a function of surface coverage.

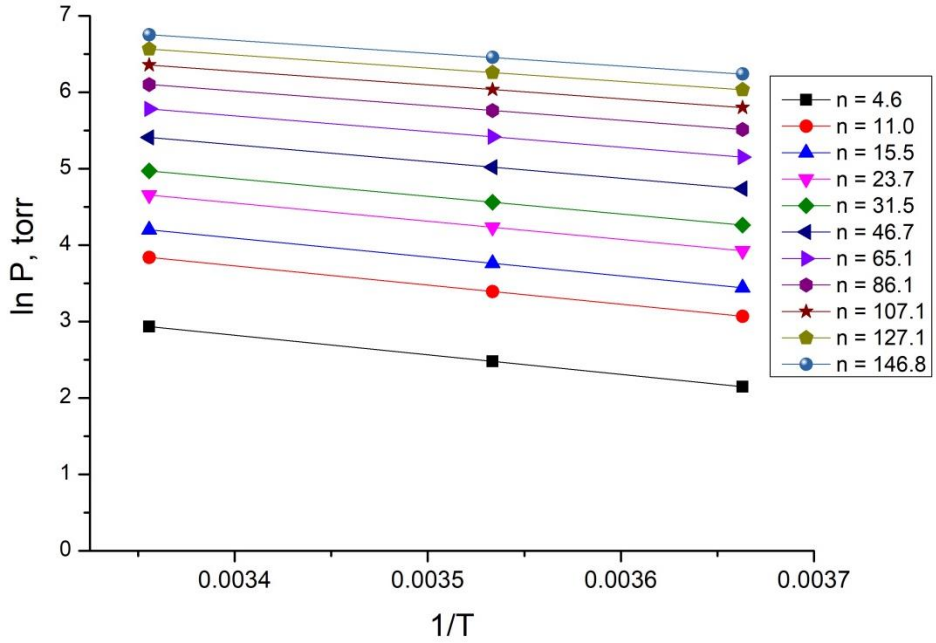

Figure S43. Isosteric lnP against 1/T plot for 273 K, 283 K and 298 K at different loadings n (in mg g^{-1}) of CO_2 in Zr-**flu**-SO_2, confirming the accuracy of the Q_{st} determined from the virial type analysis, as evidenced by the linearity in the isosters.

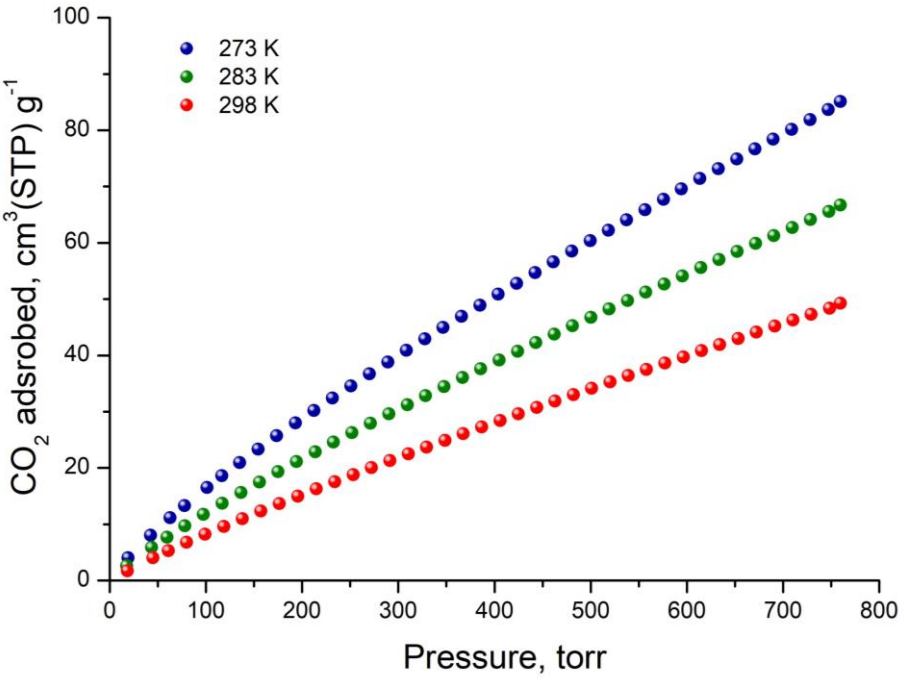

Figure S44. CO_2 adsorption isotherms of Hf-**flu**-SO_2 at 273 K, 283 K and 298 K.

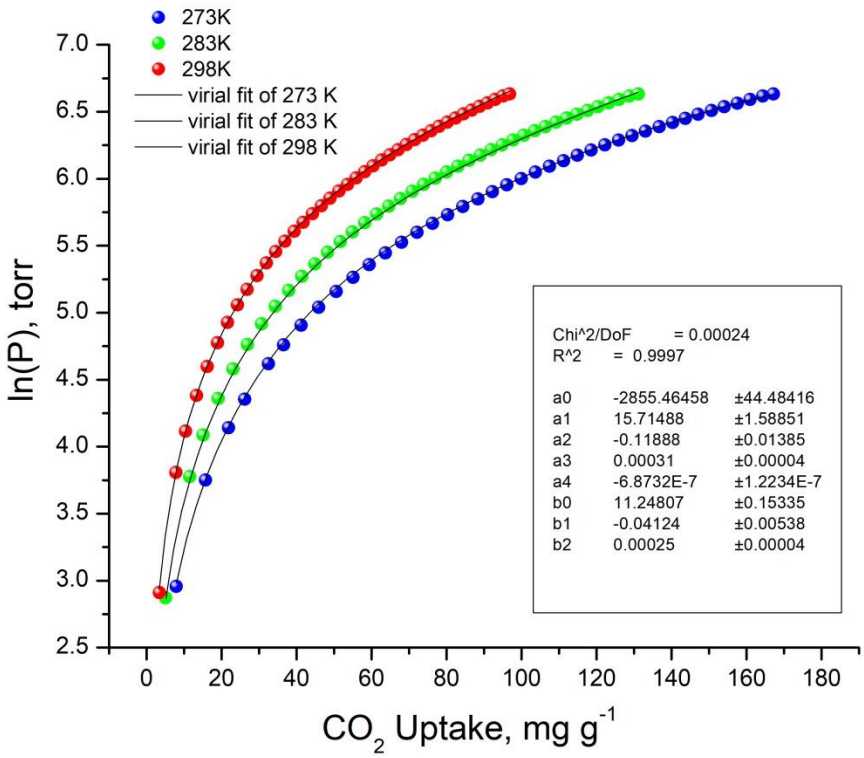

Figure S45. Virial type fitting of CO_2 adsorption isotherms of Hf-**flu**-SO_2 at 273 K, 283K and 298 K according to equation 1.

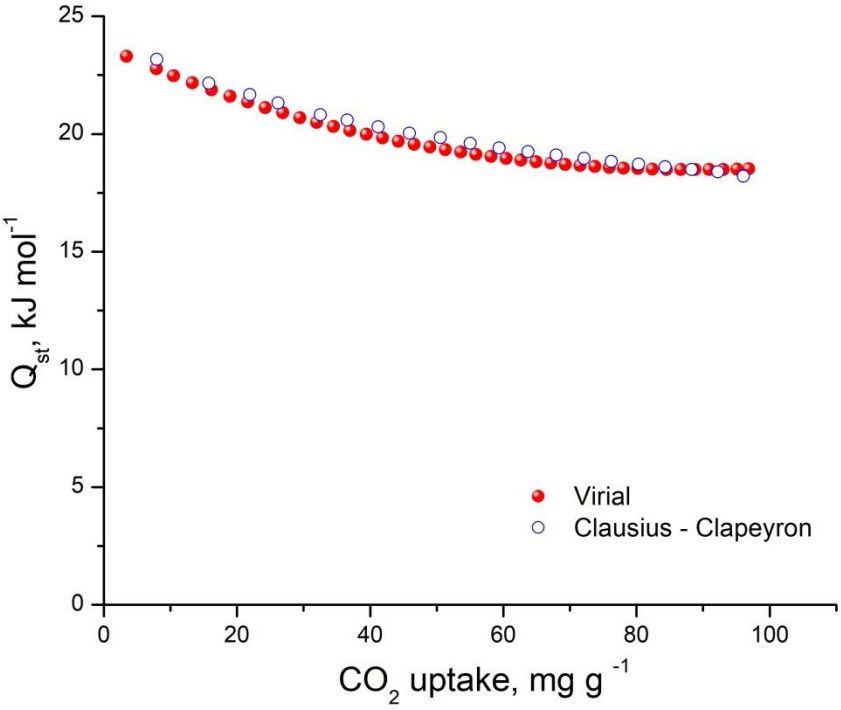

Figure S46. CO_2 isosteric heat of adsorption (Q_{st}) of Hf-**flu**-SO_2 as a function of surface coverage.

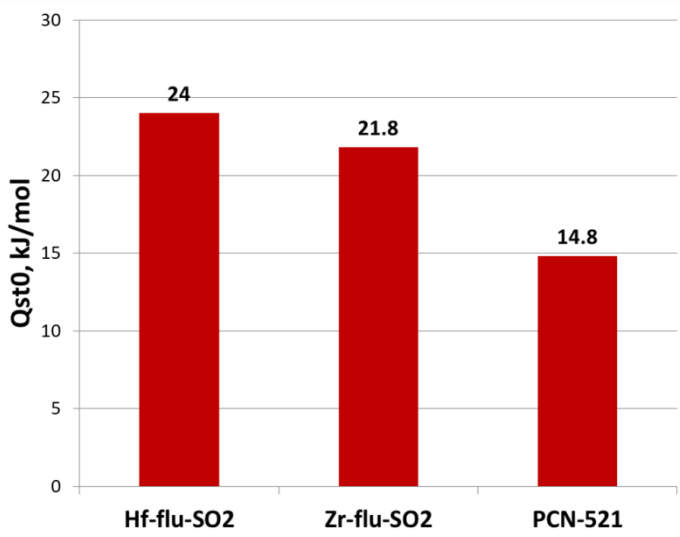

Figure S47. CO_2 Q_{st} values at zero coverage for Zr-**flu**-SO_2, Hf-**flu**-SO_2 and PCN-521.

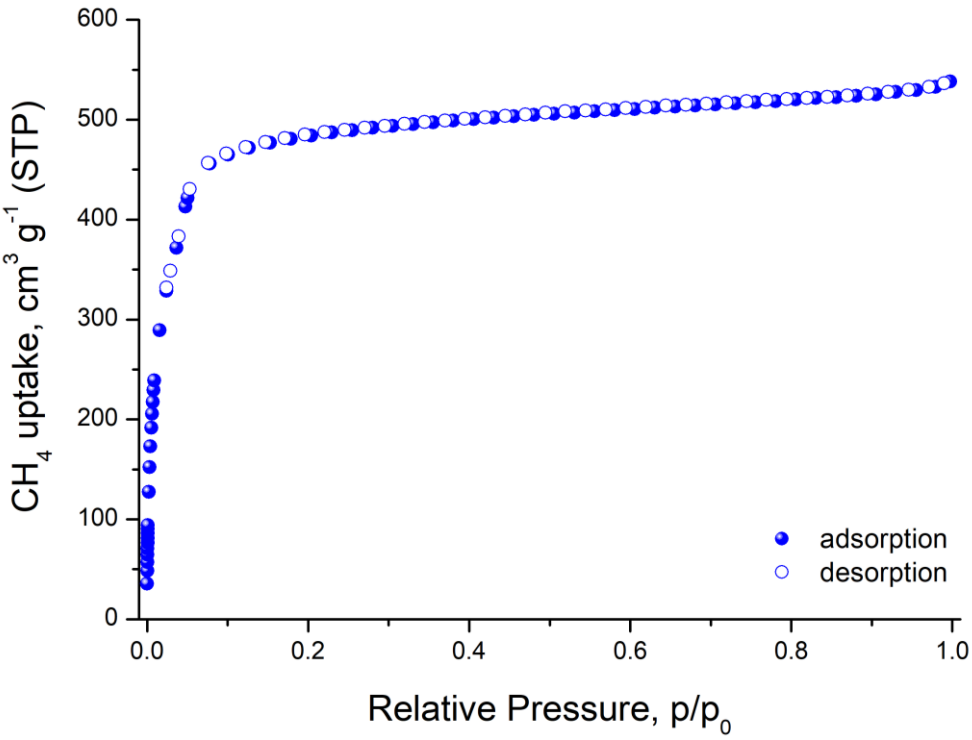

Figure S48. CH_4 sorption isotherm of the Zr-**flu**-SO_2 recorded at 112 K.

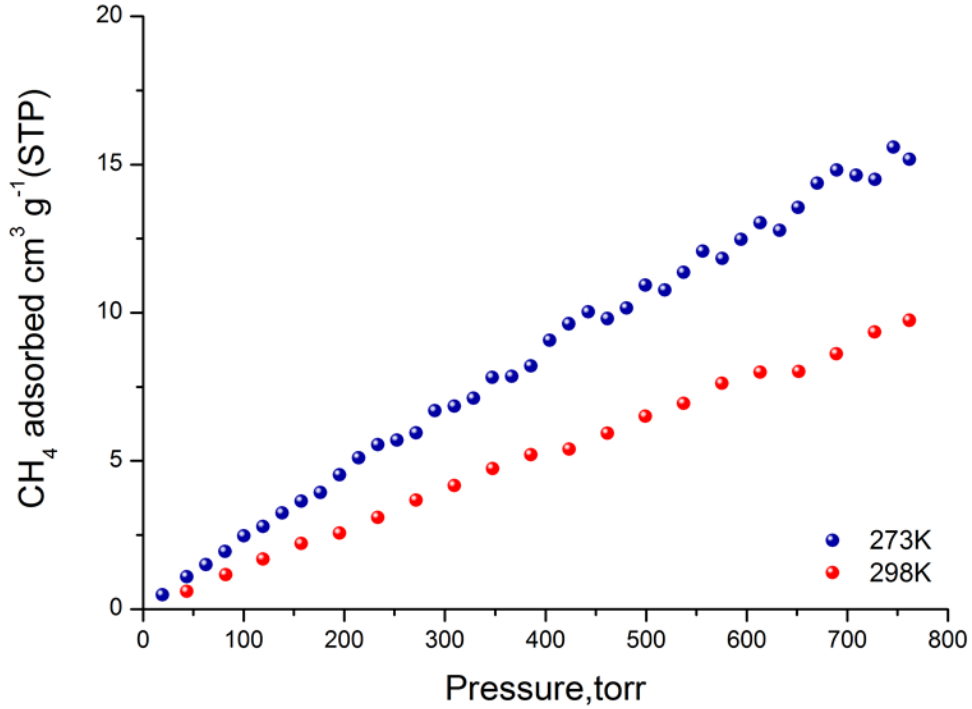

Figure S49. CH_4 adsorption isotherms of Zr-**flu**-SO_2 at 273 K and 298 K.

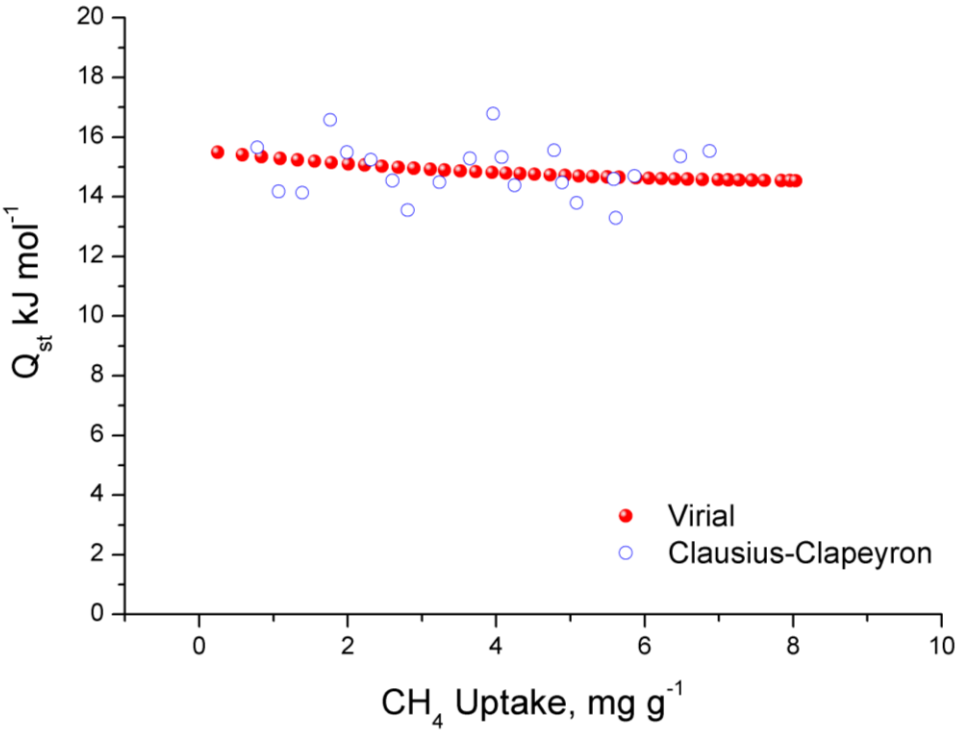

Figure S50. CH_4 isosteric heat of adsorption of Zr-**flu**-SO_2 as a function of surface coverage.

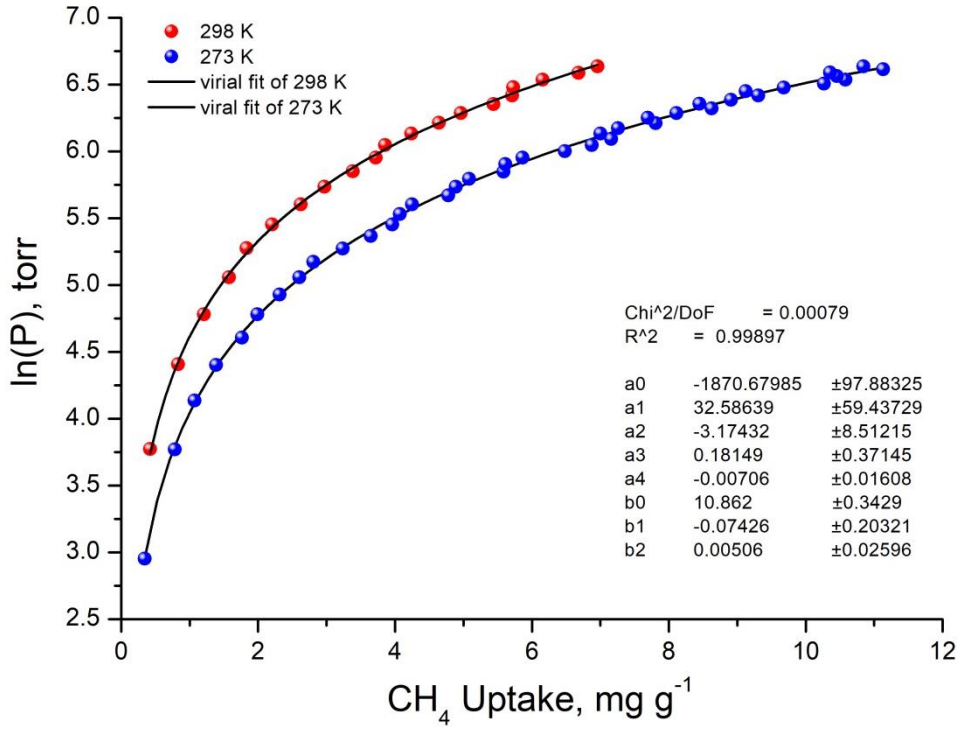

Figure S51. Virial type fitting of CH_4 adsorption isotherms of Zr-**flu**-SO_2 at 273 K and 298 K according to equation 1.

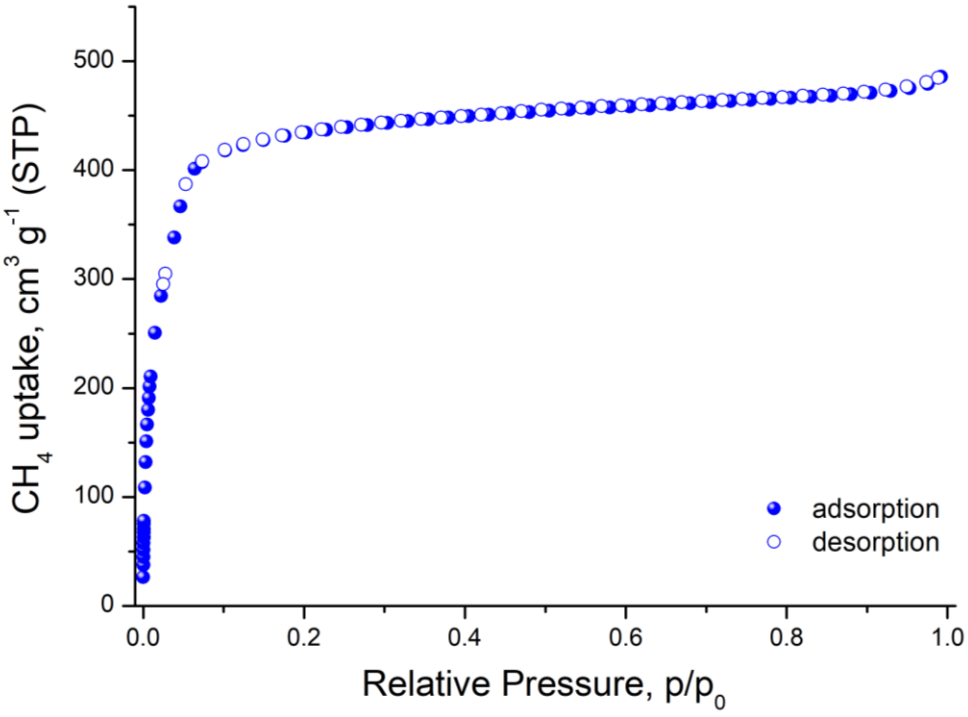

Figure S52. CH_4 sorption isotherm of the Hf-**flu**-SO_2 recorded at 112 K.

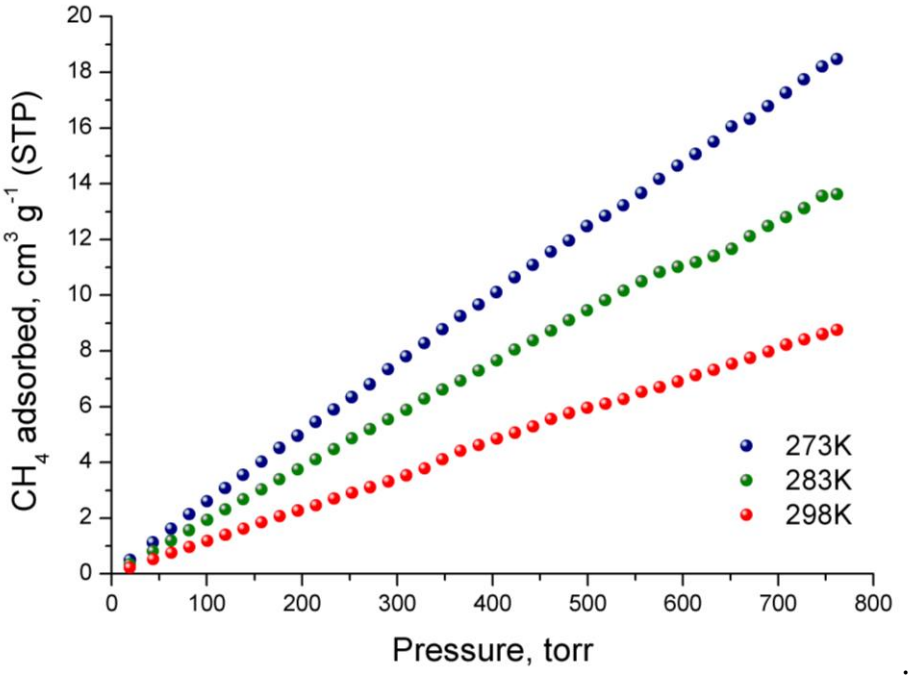

Figure S53. CH_4 adsorption isotherms of Hf-**flu**-SO_2 at 273 K, 283 K and 298 K.

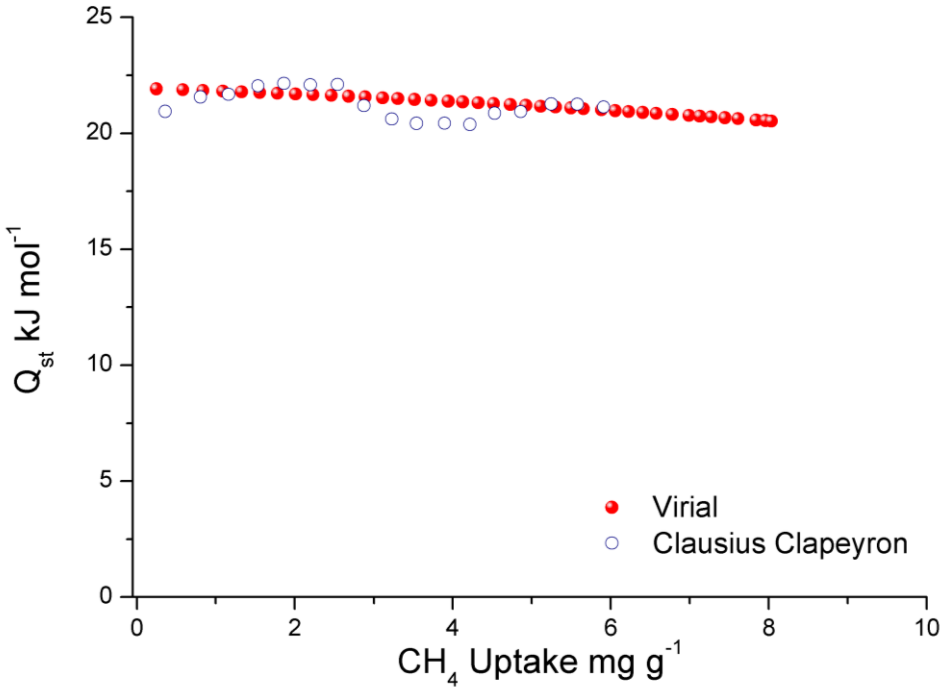

Figure S54. CH_4 isosteric heat of adsorption of Hf-**flu**-SO_2 as a function of surface coverage.

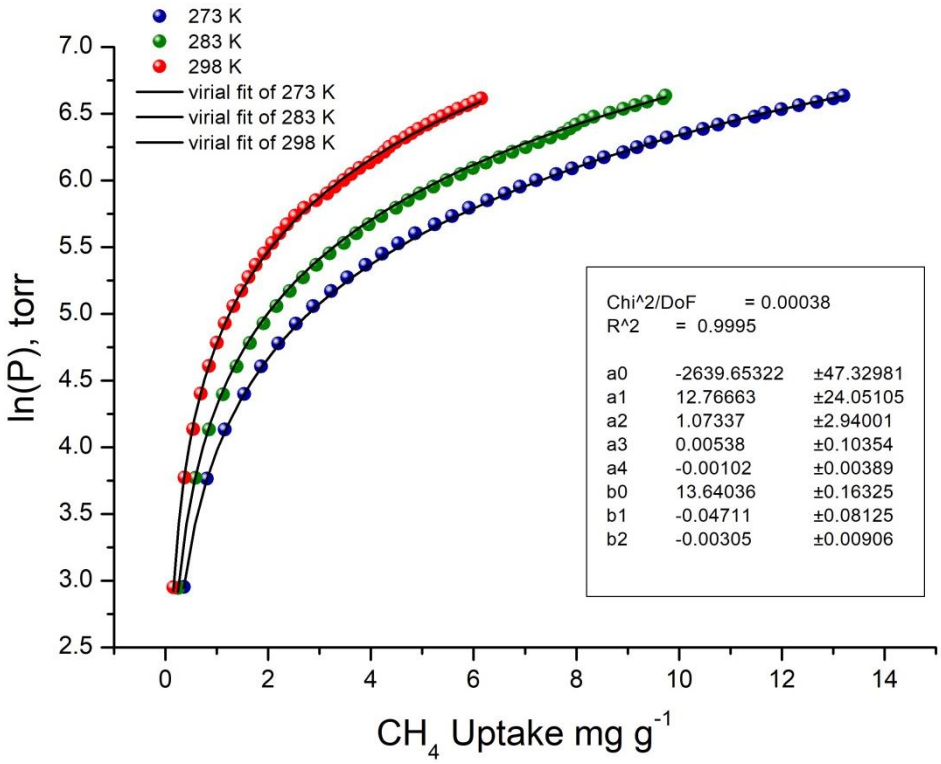

Figure S55. Virial type fitting of CH_4 adsorption isotherms of Hf-**flu**-SO_2 at 273 K, 283 K and 298 K according to equation 1.

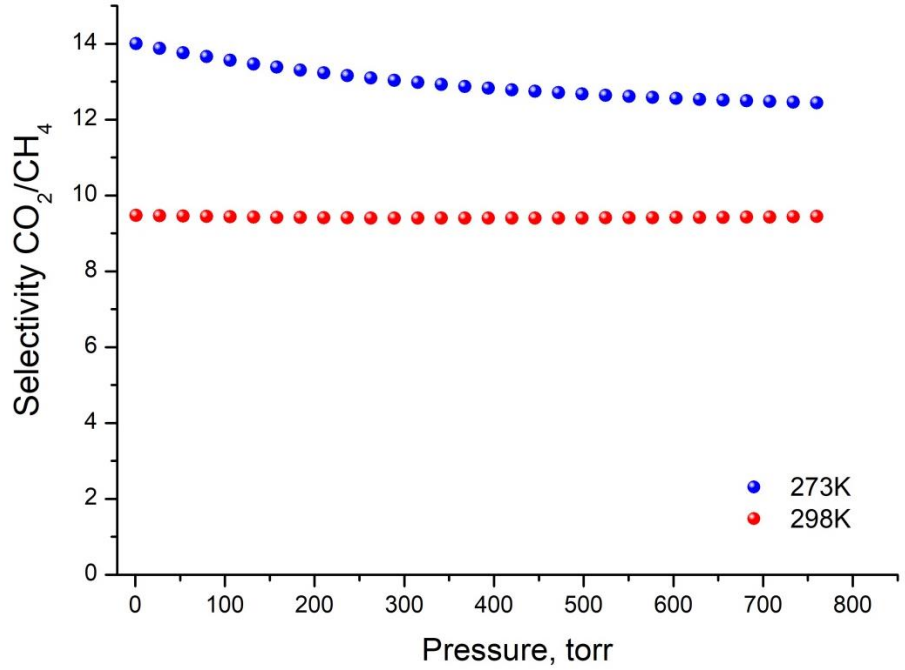

Figure S56. IAST selectivity of CO_2 over CH_4 at 273 K and 298 K for a 5/95 mixture of the Zr-**flu**-SO_2.

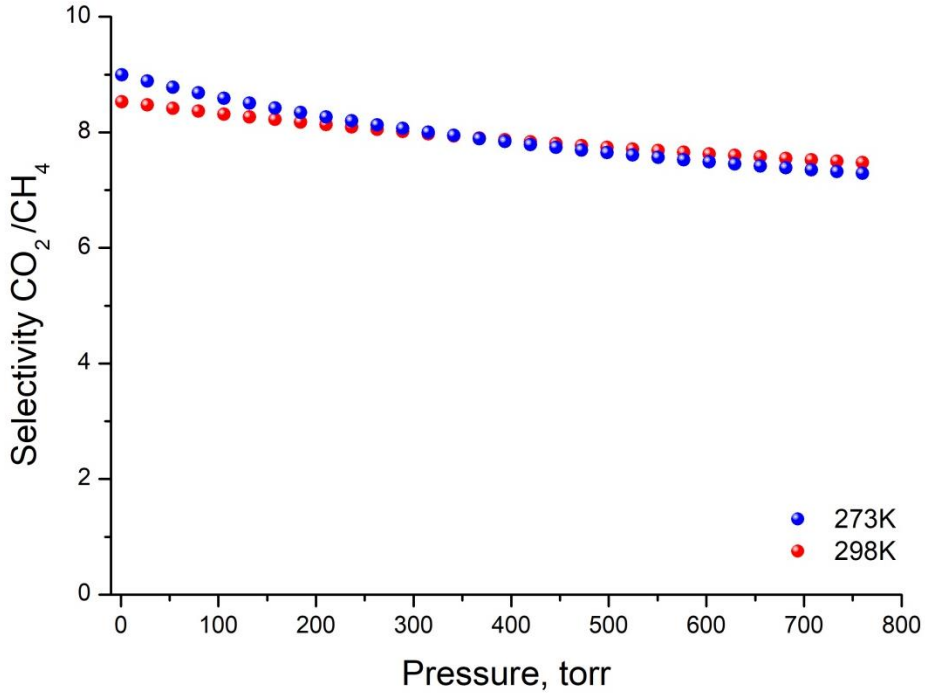

Figure S57. IAST selectivity of CO_2 over CH_4 at 273 K and 298 K for a 5/95 mixture of the Hf-**flu**-SO_2.

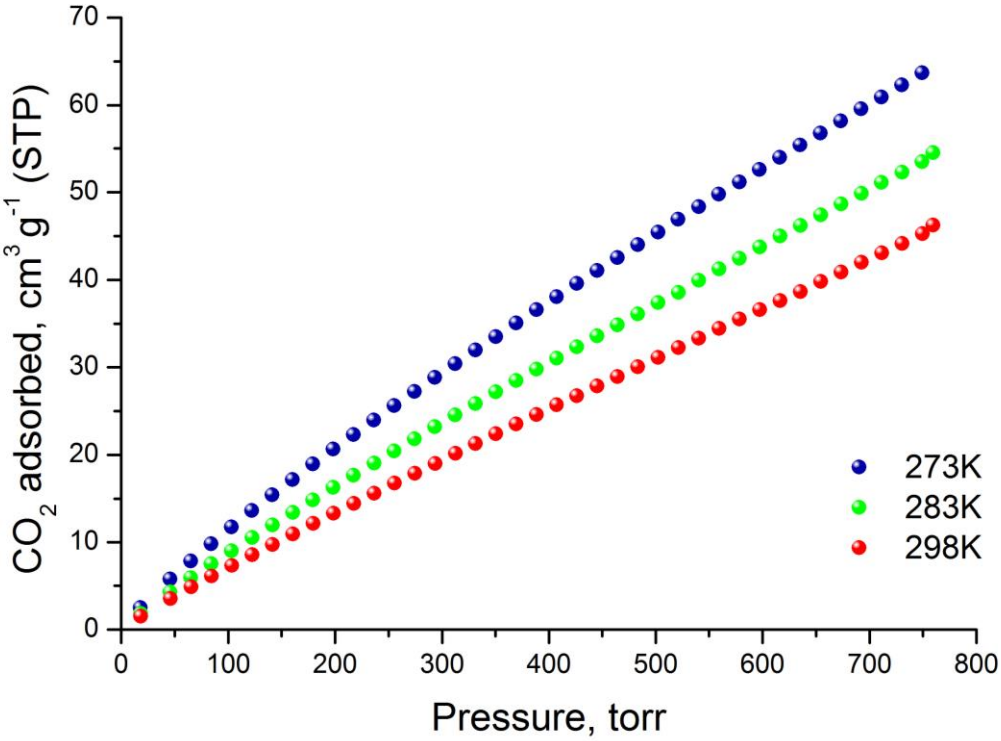

Figure S58. CO_2 adsorption isotherms of PCN-521 at 273 K, 283 K and 298 K.

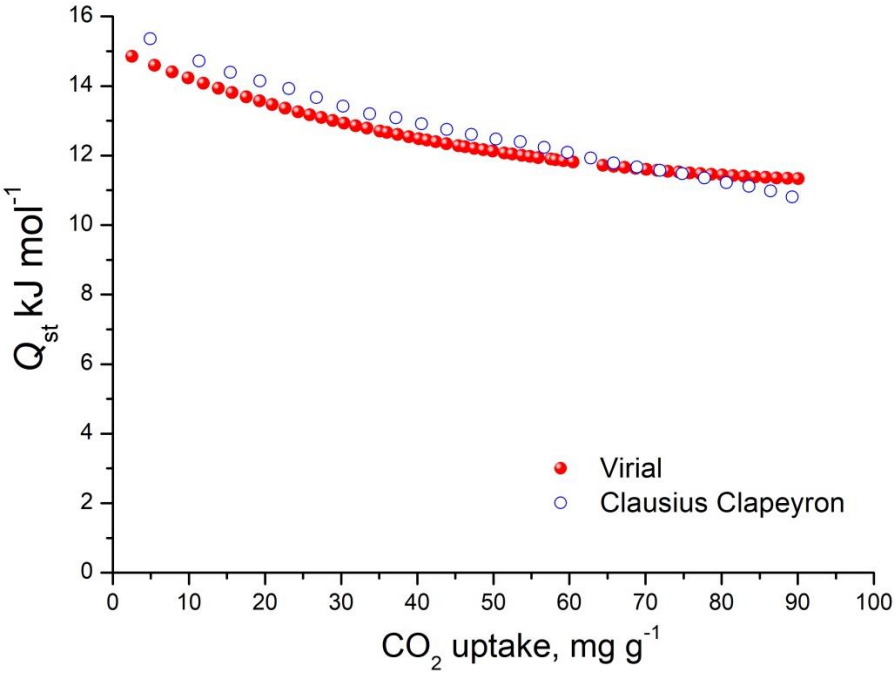

Figure S59. CO_2 isosteric heat of adsorption of PCN-521 as a function of surface coverage.

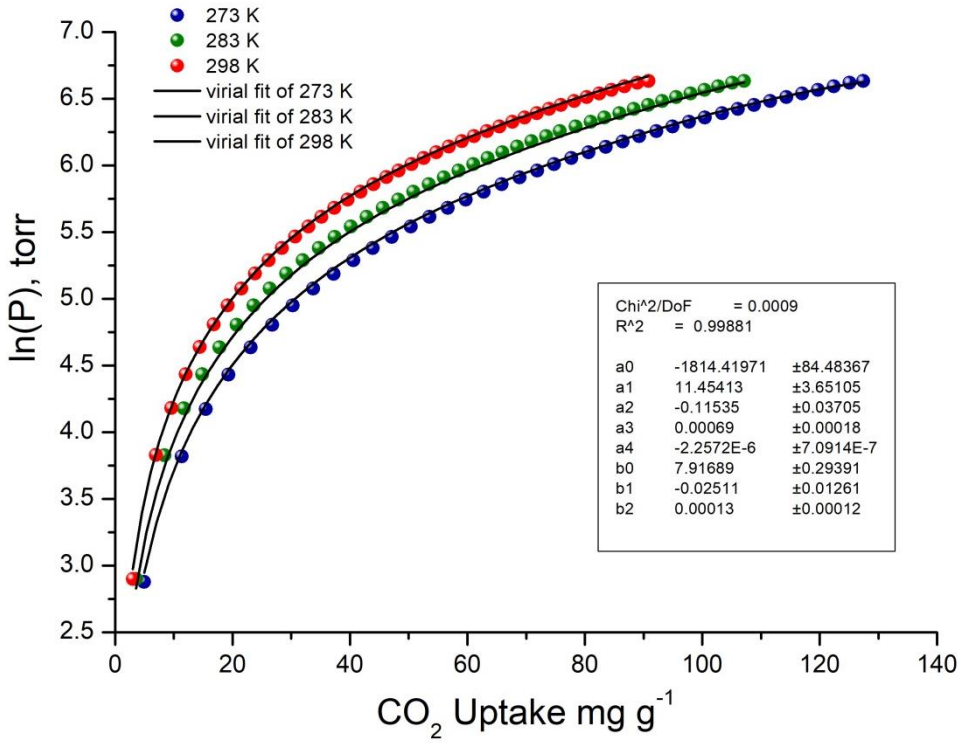

Figure S60. Virial type fitting of CO_2 adsorption isotherms of PCN-521 at 273 K, 283 K and 298 K according to equation 1.

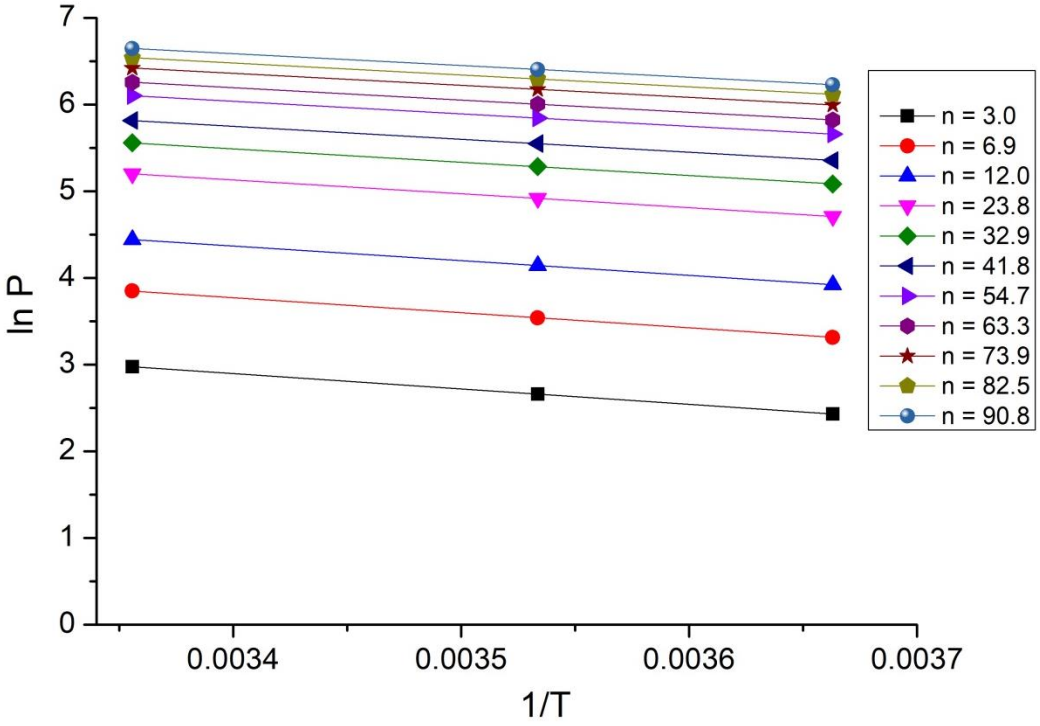

Figure S61. Isosteric lnP against 1/T plot for 273 K, 283 K and 298 K at different loadings n (in mg g^{-1}) of CO_2 in PCN-521, confirming the accuracy of the Q_{st} determined from the virial type analysis, as evidenced by the linearity in the isosters.

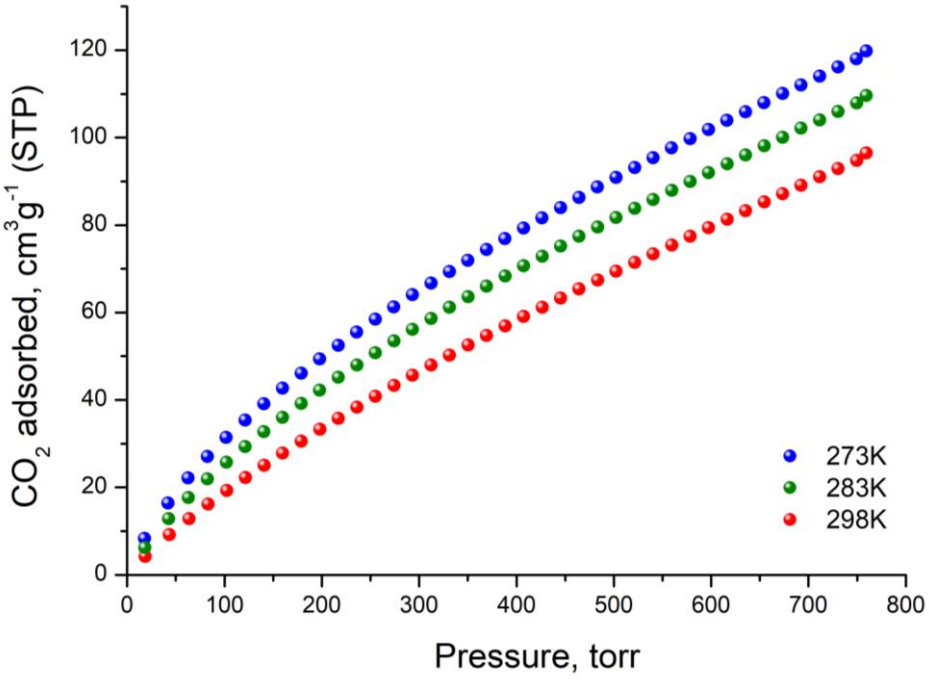

Figure S62. CO_2 adsorption isotherms of Y-**hpt**-MOF-1 at 273 K, 283 K and 298 K.

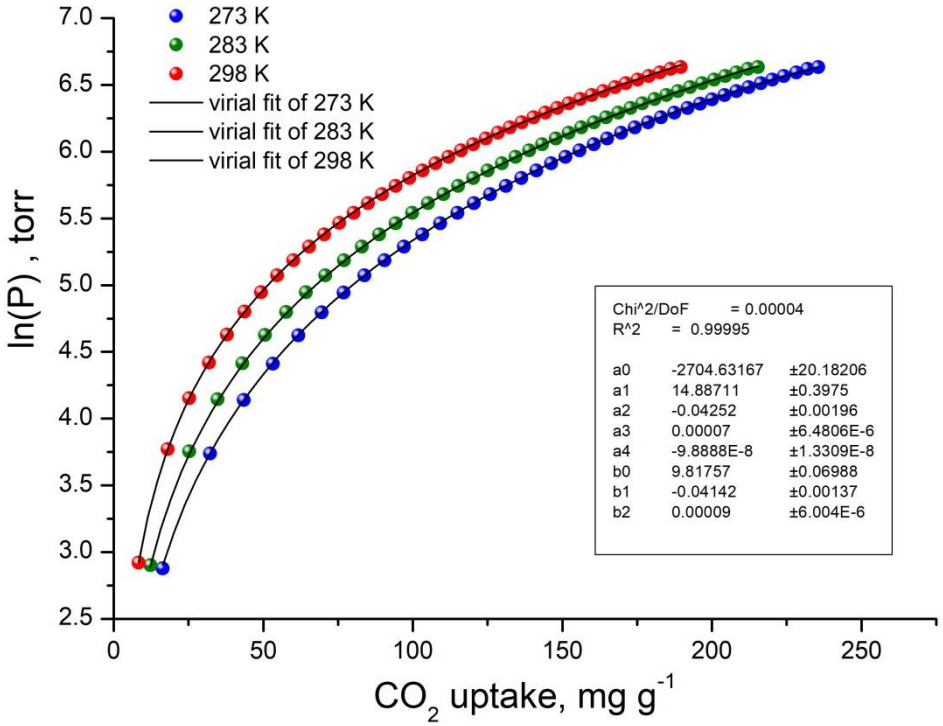

Figure S63. Virial type fitting of CO_2 adsorption isotherms of Y-**hpt**-MOF-1 at 273 K, 283 K and 298 K according to equation 1.

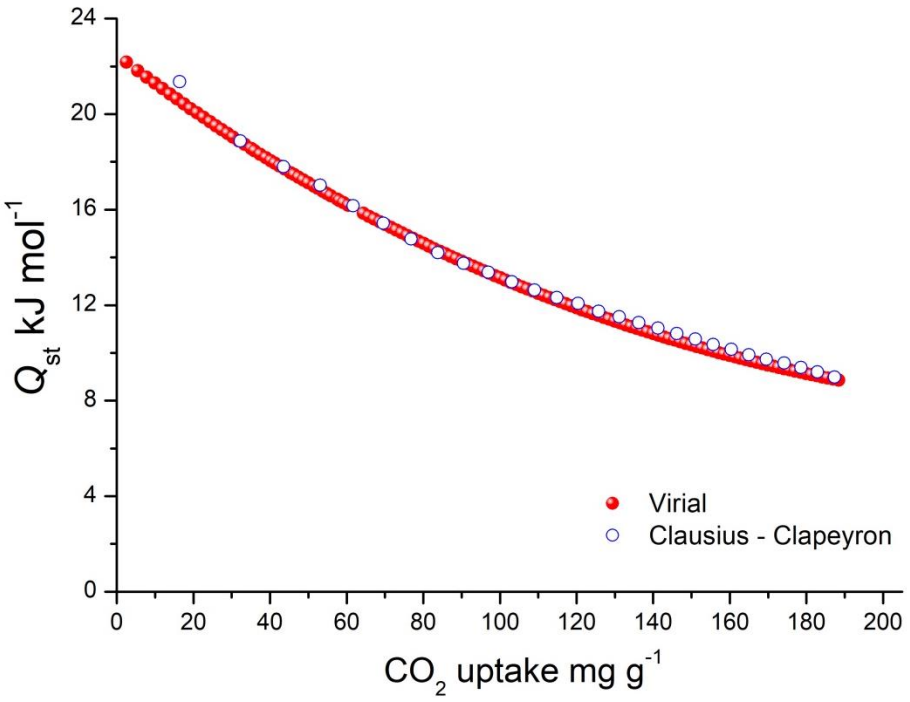

Figure S64. CO_2 isosteric heat of adsorption of Y-**hpt**-MOF-1 as a function of surface coverage.

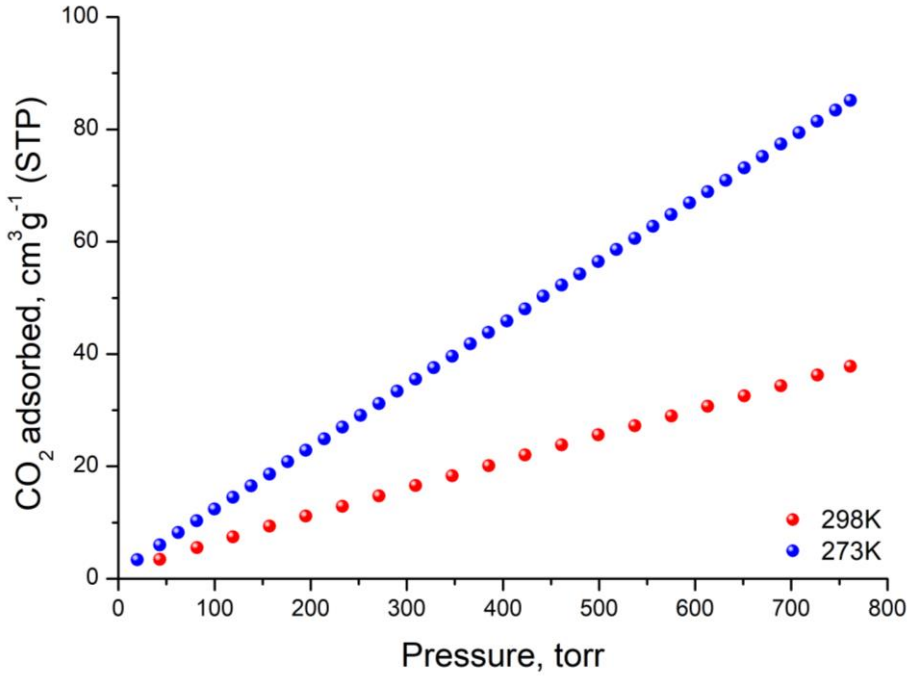

Figure S65. CO_2 adsorption isotherms of Y-**ken**-MOF-1 at 273 K and 298 K.

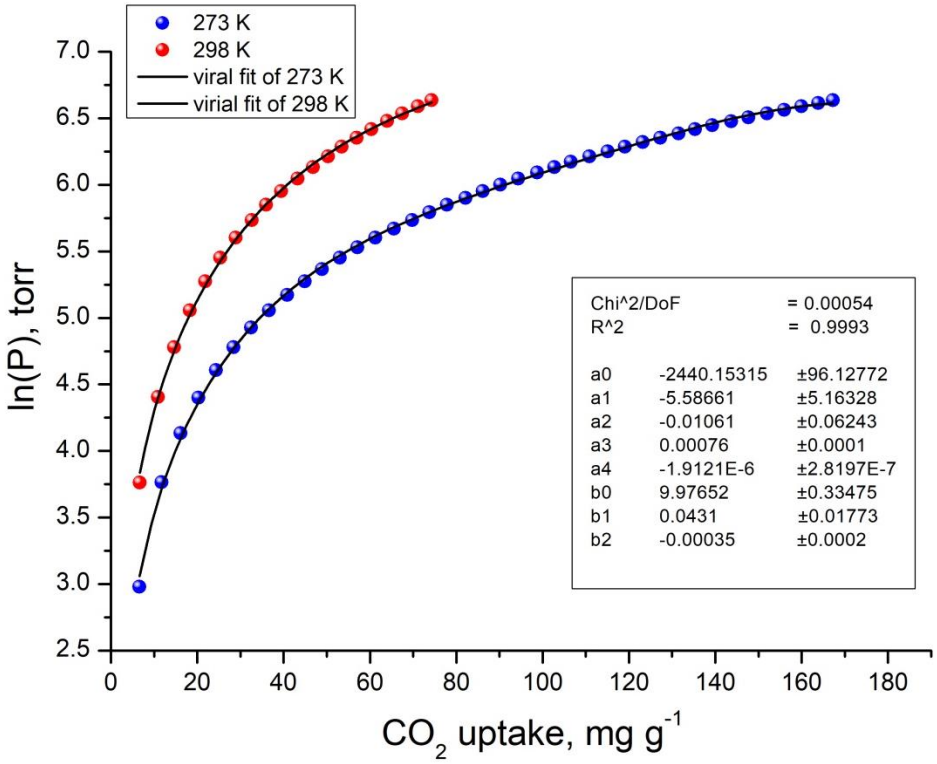

Figure S66. Virial type fitting of CO_2 adsorption isotherms of Y-**ken**-MOF-1 at 273 K and 298 K according to equation 1.

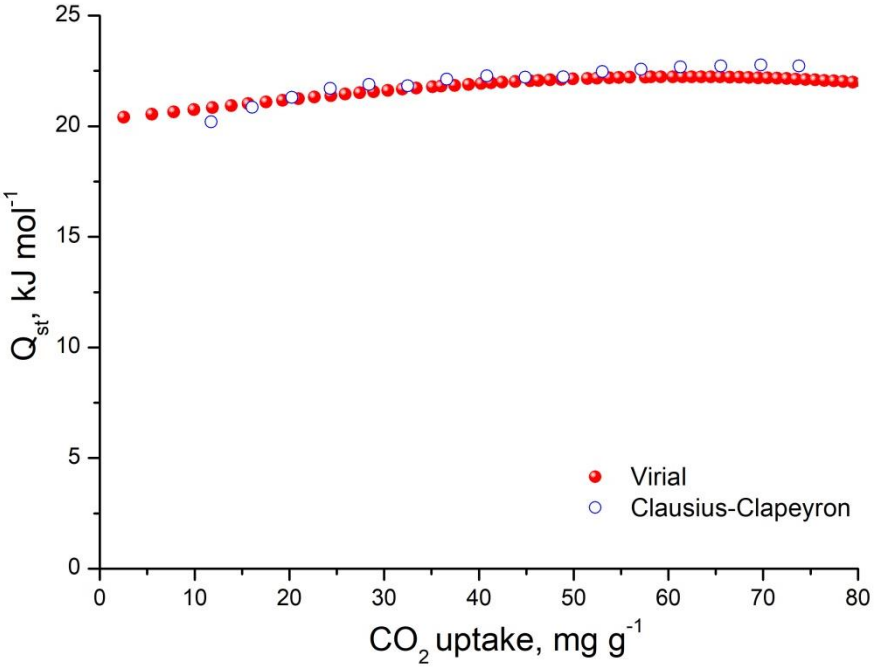

Figure S67. CO_2 isosteric heat of adsorption of Y-**ken**-MOF-1 as a function of surface coverage.

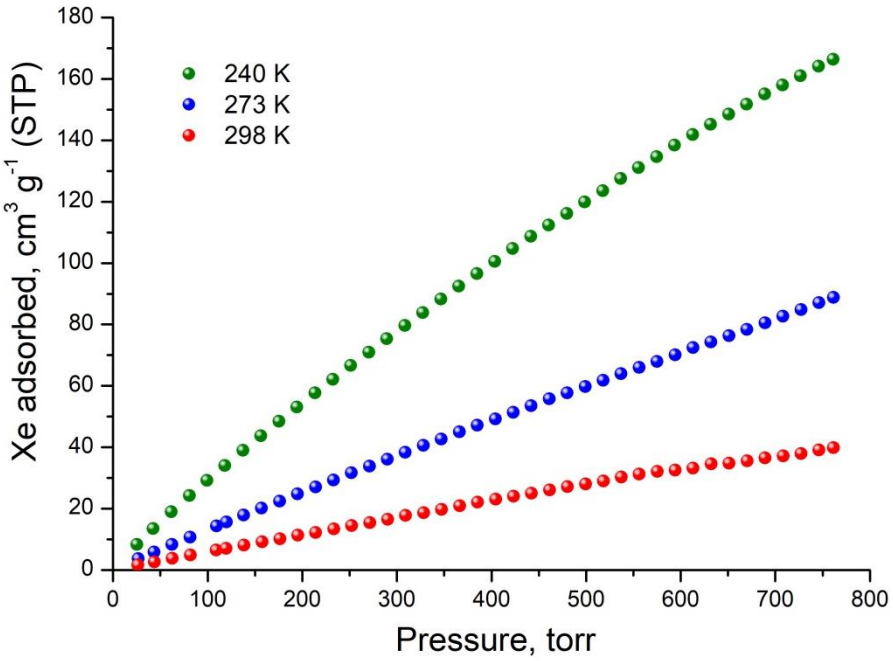

Figure S68. Xe adsorption isotherms of Y-**ken**-MOF-1 at 240 K, 273 K and 298 K up to 1 bar.

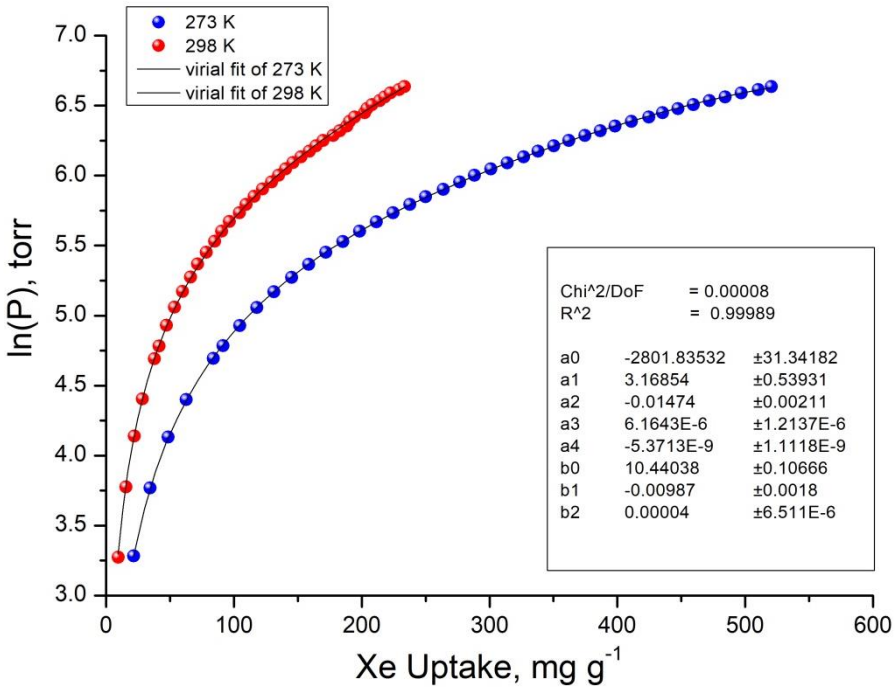

Figure S69. Virial type fitting of Xe adsorption isotherms of Y-**ken**-MOF-1 at 273 K and 298K according to equation 1.

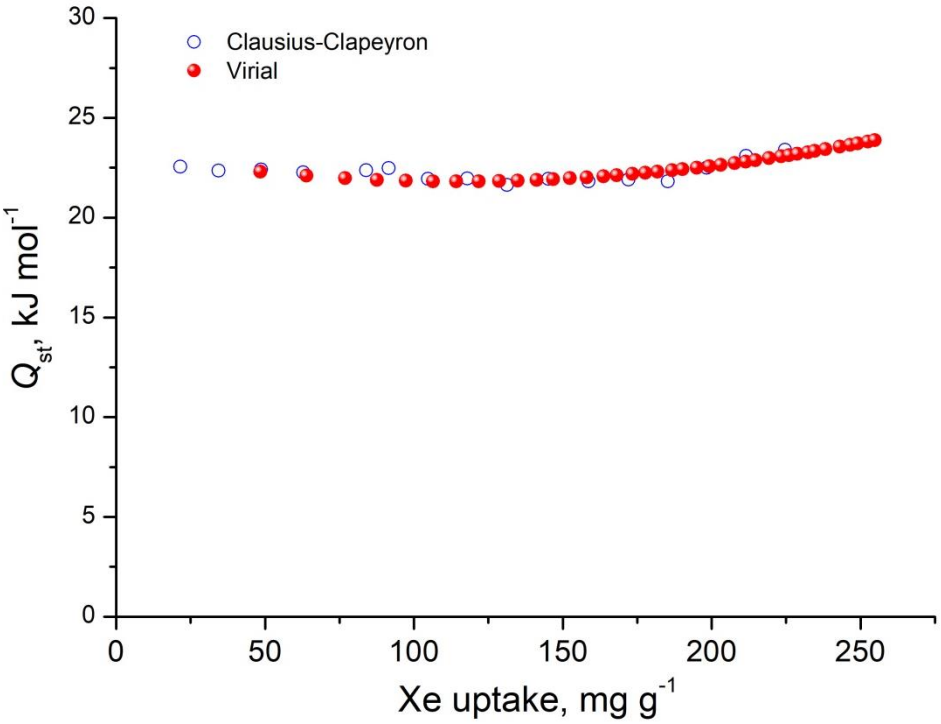

Figure S70. Xe isosteric heat of adsorption of Y-**ken**-MOF-1 as a function of surface coverage.

NMR measurements of acid digested samples

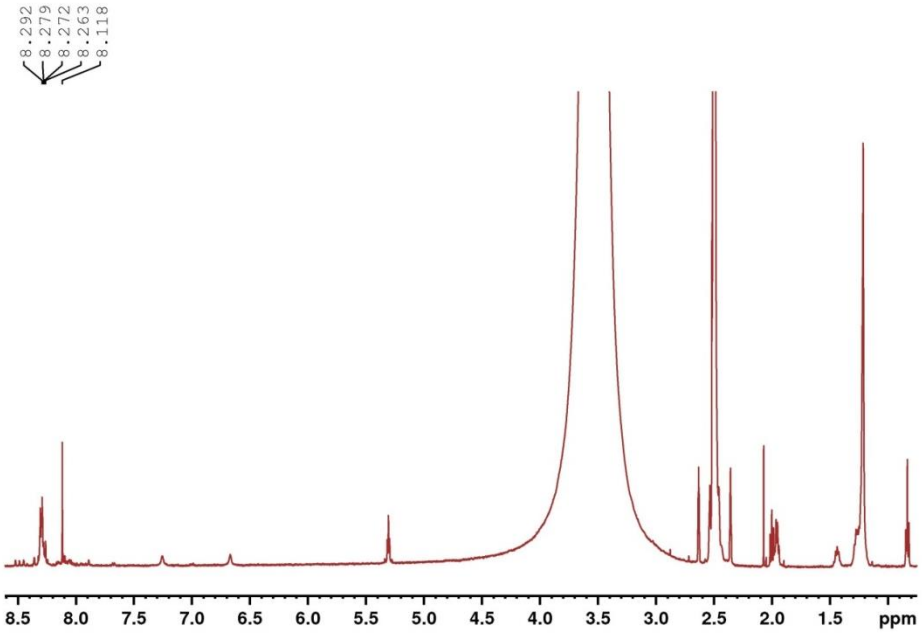

Figure S71. ^{1}H NMR spectrum of evacuated Zr-**flu**-SO_2 after digesting the sample in HF/DMSO-d_6 solution.

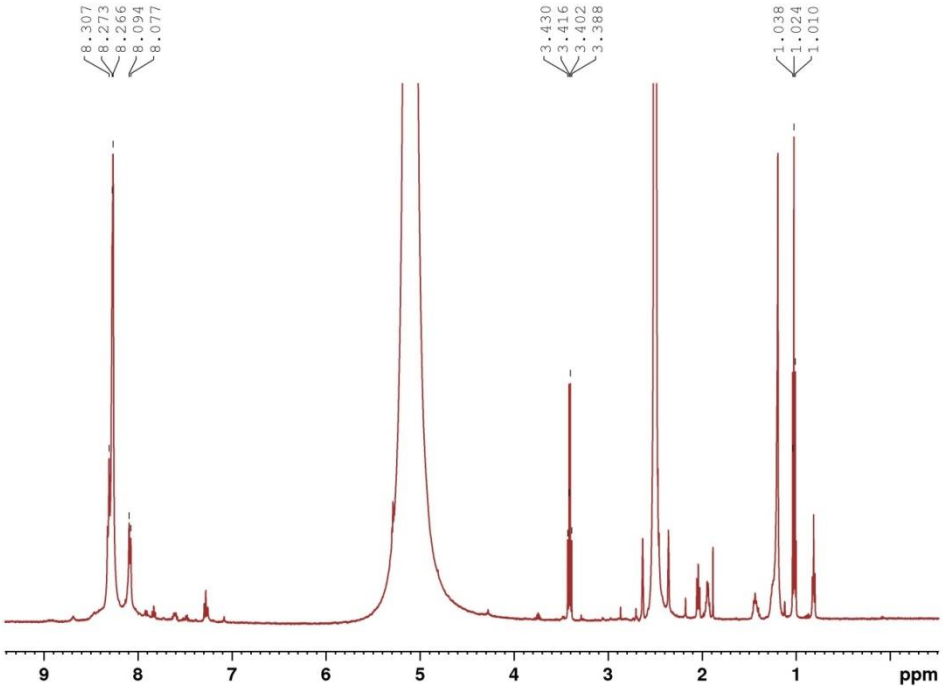

Figure S72. ^{1}H NMR spectrum of evacuated Y-**hpt**-MOF-1 after digesting the sample in HCl/DMSO-d_6 solution.

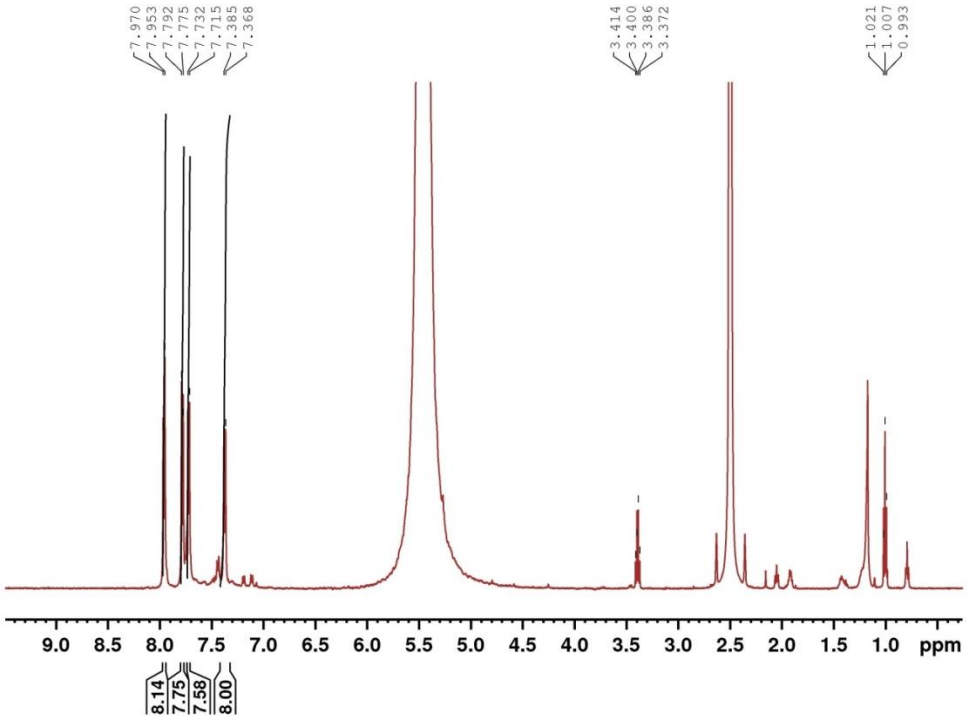

Figure S73. ^{1}H NMR spectrum of evacuated Y-**ken**-MOF-1 after digesting the sample in HCl/DMSO-d_6 solution.

Thermal gravimetric analyses (TGA)

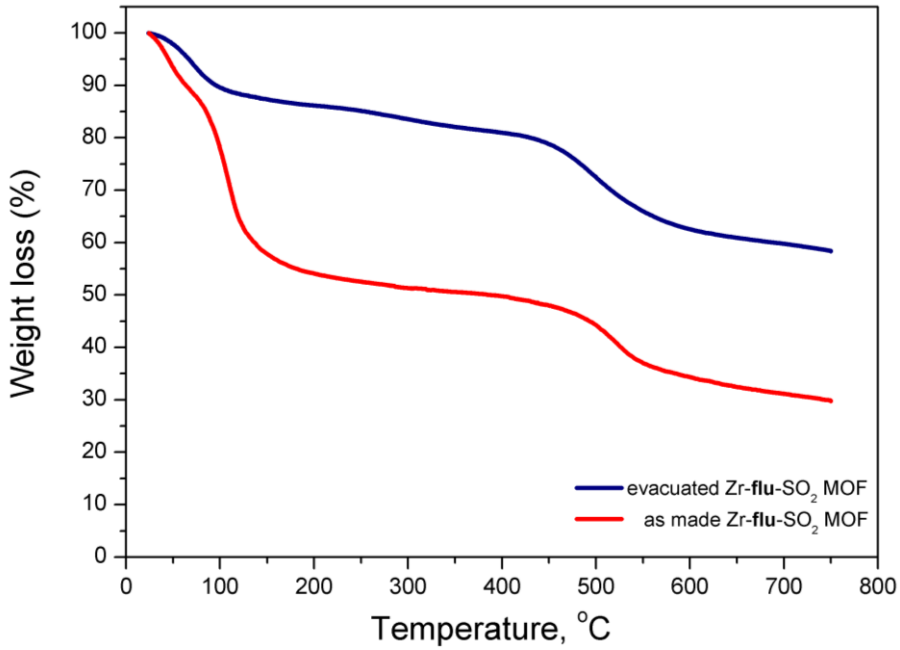

Figure S74. TGA curve for the as-made (red) Zr-**flu**-SO_2 and the corresponding evacuated (blue) solid, recorded under nitrogen flow with a heating rate 5 deg/min.

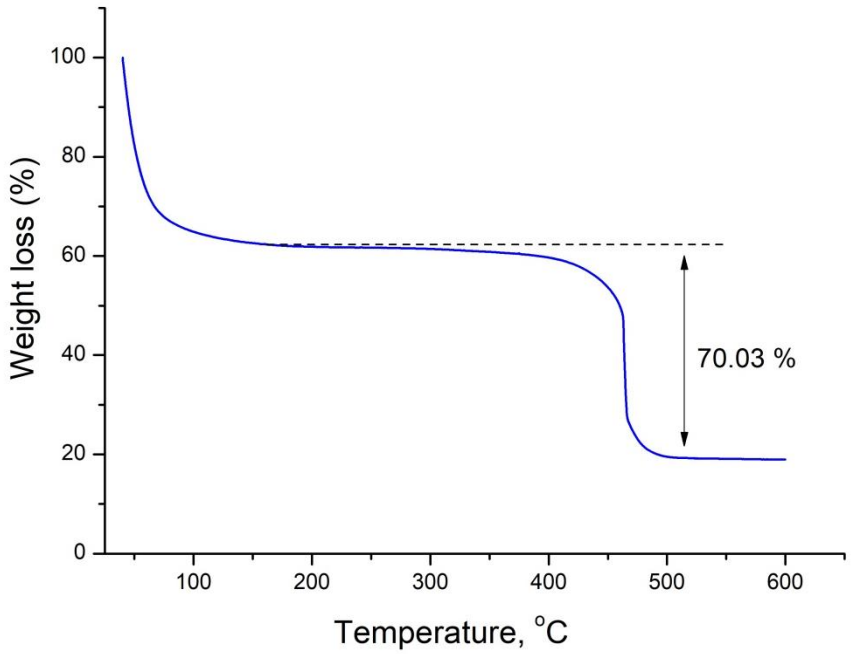

Figure S75. TGA curve of an ethanol exchanged Y-**ken**-MOF-1 recorded under air flow with a heating rate 5 deg/min. The observed weight loss between 130 °C (plateau after the removal of excess ethanol) and 600 °C is 70.03 % which is higher compared to the expected weight loss of 64.50 % based on the chemical formula $Y_9(\mu_3\text{-}O)_2(\mu_3\text{-}OH)_{12}(OH)_2(H_2O)_{11}\mathbf{L}_2$ and considering the formation of Y_2O_3 at 600 °C under air. The observed 5.5 % increase in weight loss could be associated with the presence of an amount of trapped unreacted ligand inside the pore space of Y-**ken**-MOF-1. This increase corresponds to **2.65** ligands per formula unit instead of **2**. The corresponding IR spectra shows a broad shoulder at 1683 cm^{-1} which is associated with the stretching vibration of the C=O bond of the free ligand. (see below).

Infrared Spectroscopy

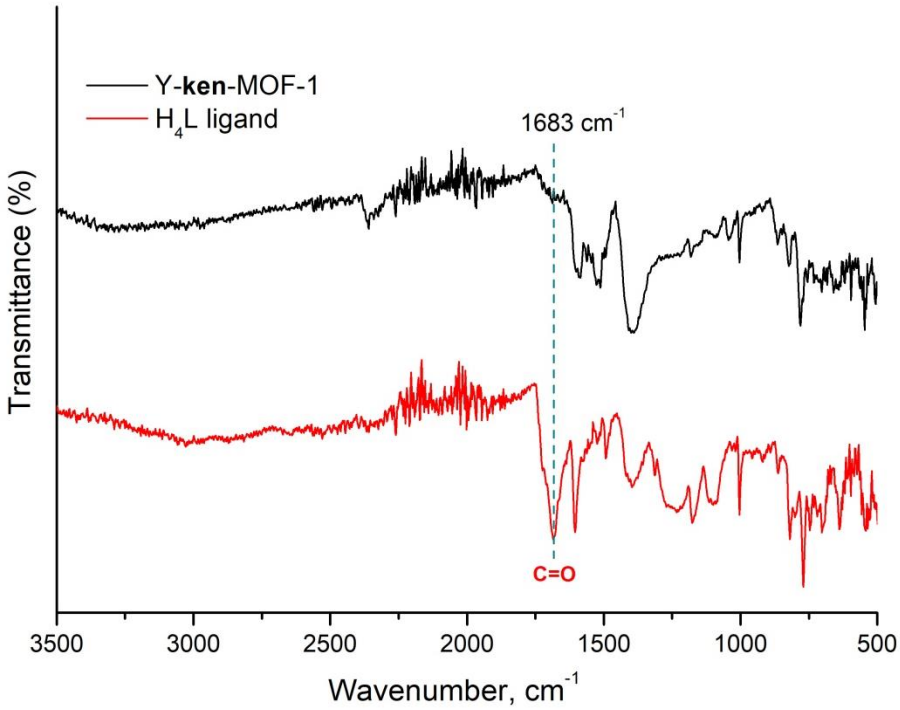

Figure S76. ATR-IR spectrum of ethanol exchanged Y-**ken**-MOF-1 and the free ligand $H_4\mathbf{L}$.

References

(1) Ma, L. Q.; Jin, A.; Xie, Z. G.; Lin, W. B., Freeze Drying Significantly Increases Permanent Porosity and Hydrogen Uptake in 4,4-Connected Metal-Organic Frameworks. *Angew. Chem. Int. Ed.* **2009,** *48* (52), 9905-9908.
(2) Zhang, M. W.; Chen, Y. P.; Bosch, M.; Gentle, T.; Wang, K. C.; Feng, D. W.; Wang, Z. Y. U.; Zhou, H. C., Symmetry-Guided Synthesis of Highly Porous Metal-Organic Frameworks with Fluorite Topology. *Angew. Chem. Int. Ed.* **2014,** *53* (3), 815-818.
(3) Hu, F.; Di, Z.; Wu, M.; Hong, M.; Li, J., A Robust Multifunctional Eu6-Cluster Based Framework for Gas Separation and Recognition of Small Molecules and Heavy Metal Ions. *Cryst. Growth Des.* **2019,** *19* (11), 6381-6387.
(4) Guillerm, V.; Kim, D.; Eubank, J. F.; Luebke, R.; Liu, X.; Adil, K.; Lah, M. S.; Eddaoudi, M., A supermolecular building approach for the design and construction of metal–organic frameworks. *Chem. Soc. Rev.* **2014,** *43* (16), 6141-6172.
(5) Wei, N.; Zhang, Y.; Liu, L.; Han, Z. B.; Yuan, D. Q., Pentanuclear Yb(III) cluster-based metal-organic frameworks as heterogeneous catalysts for CO2 conversion. *Appl. Catal. B-Environ.* **2017,** *219*, 603-610.
(6) He, Y.; Furukawa, H.; Wu, C.; O'Keeffe, M.; Chen, B., A mesoporous lanthanide–organic framework constructed from a dendritic hexacarboxylate with cages of 2.4 nm. *CrystEngComm* **2013,** *15* (45), 9328-9331.
(7) Sumida, K.; Rogow, D. L.; Mason, J. A.; McDonald, T. M.; Bloch, E. D.; Herm, Z. R.; Bae, T. H.; Long, J. R., Carbon Dioxide Capture in Metal-Organic Frameworks. *Chem. Rev.* **2012,** *112* (2), 724-781.
(8) Czepirski, L.; Jagiello, J., VIRIAL-TYPE THERMAL EQUATION OF GAS SOLID ADSORPTION. *Chem. Eng. Sci.* **1989,** *44* (4), 797-801.
(9) Myers, A. L.; Prausnitz, J. M., Thermodynamics of mixed-gas adsorption. *AIChE Journal* **1965,** *11* (1), 121-127.
(10) Bae, Y.-S.; Mulfort, K. L.; Frost, H.; Ryan, P.; Punnathanam, S.; Broadbelt, L. J.; Hupp, J. T.; Snurr, R. Q., Separation of CO2 from CH4 Using Mixed-Ligand Metal−Organic Frameworks. *Langmuir* **2008,** *24* (16), 8592-8598.
(11) Armatas, G. S.; Kanatzidis, M. G., Mesoporous germanium-rich chalcogenido frameworks with highly polarizable surfaces and relevance to gas separation. *Nat. Mater.* **2009,** *8* (3), 217-222.